The University of Sydney
Department of Civil Engineering
Sydney NSW 2006
AUSTRALIA

http://www.civil.usyd.edu.au/

Centre for Advanced Structural Engineering

Compression Tests of DuraGal Angles Loaded Parallel With a Leg

Research Report No. R799

By

Dan Popovic, BSc, BE,
Gregory J. Hancock, BSc, BE, PhD
Kim J. R. Rasmussen, MSciEng, PhD

March 2000

Copyright Notice

Department of Civil Engineering, Research Report R799
Compression Tests of DuraGal Angles Loaded Parallel With a Leg

D.Popovic@civil.usyd.edu.au
G.Hancock@civil.usyd.edu.au
K.Rasmussen@civil.usyd.edu.au

Published by:
Department of Civil Engineering
The University of Sydney
Sydney, NSW, 2006
AUSTRALIA

March 2000

http://www.civil.usyd.edu.au

COMPRESSION TESTS OF DURAGAL ANGLES LOADED PARALLEL WITH A LEG

Dan Popovic, BSc, BE,
Gregory J. Hancock, BSc, BE, PhD
and
Kim J. R. Rasmussen, MSciEng, PhD

Research Report No. R799
March 2000

Synopsis

This report presents the results of 11 compression tests performed on cold-formed, in-line galvanised, slender 50x50x2.5 DuraGal equal angles. The angles were tested between pinned ends and loaded axially with eccentric load which caused bending parallel with a leg at the ends. Tests were performed over a range of lengths to produce column strength curves. The sensitivity to load eccentricity was investigated by applying the load at the centroid, at a leg and at a point outside the section. Detailed measurements of material properties, residual stresses and geometric imperfections were conducted.

The test data are compared with the design rules of the Australian Standards for Cold-Formed (AS/NZS 4600-1996) and Hot-Rolled (AS 4100-1998) Steel Structures as well as the American Iron and Steel Institute (AISI-1997) Specification for the Design of Cold-formed Steel Structural Members, the American Society of Civil Engineers Standard (ASCE-1991) for the Design of Latticed Steel Transmission Structures and the American Institute of Steel Construction (AISC-1993) Specification for Load and Resistance Factor Design of Single-Angle Members. Recommendations on the application of these design rules to cold-formed angles are included in the paper.

The test results show that the design rules of both Australian standards and the AISI and AISC specifications are conservative. The conservatism is most pronounced at short lengths. Improved design rules for AS/NZS 4600 and the AISI Specification are suggested. The design rules of the ASCE Standard are in fairly good agreement with the tests.

Contents

COMPRESSION TESTS OF DURAGAL ANGLES LOADED PARALLEL WITH A LEG

1. Introduction

Steel angles are used extensively as chord and web members of trusses, as leg and diagonal members of latticed transmission line towers, and as bracing members for lateral support of beams and columns, among other applications. Traditionally, hot-rolled angles were used in these applications but in recent years cold-formed angles have become more popular because their higher strength and lighter weight lead to cost reductions in the construction industry. Angles are widely used because of their simple geometry and ease of connection. At the same time, angles can be amongst the most difficult sections to design, especially when they are eccentrically loaded due to attachment as shown in Fig. 1.

This research report presents the second stage of the Australian Research Council Collaborative Research Project entitled "Behaviour and Design of Galvanised Cold-Formed Steel Structural Members". It contains the results of a series of compression tests performed on cold-formed DuraGal angles with a nominal yield stress of 400 MPa manufactured by BHP Structural and Pipeline Products (BHP-SPP). The specimens were supported such that they were free to rotate at their ends about an axis parallel with a leg, while the perpendicular rotation and the twist rotation were restrained. The test arrangement typically simulated web members of trusses where angles are connected by one leg. The first stage of the research project was reported in Popovic et al. (1999) and concerned the strength of angle columns loaded at the ends by axial force to produce bending about the minor principal axis. The present research program is distinct from previous research programs on cold-formed angles in that the sections were in-line galvanised. This process accelerates the strain-ageing and leads to enhanced yield stress values immediately after the forming process.

The objective of this report is to provide test data for angles loaded parallel with a leg and to compare the data with the design rules for cold-formed angles in the Australian Limit States Steel Structures Standard AS 4100-1998 (Standards Australia 1998), the Australian/New Zealand Standard for Cold-Formed Steel Structures AS/NZS AS4600-1996 (Standards Australia 1996), the American Iron and Steel Institute (1997) Specification for the Design of Cold-formed Steel Structural Members, the American Society of Civil Engineers (1991) Standard for the Design of Latticed Steel Transmission Structures and the American Institute of Steel Construction (1993) Specification for Load and Resistance Factor Design of Single-Angle Members. Recommendations on the

applicability of the design rules of these specifications to cold-formed angles are included in the report. A further objective is to investigate the sensitivity to loading eccentricity by varying the loading position relative to the centroid. The loading points chosen were at the centroid, at the leg parallel to the bending axis and at a point outside the section.

2. Material properties

2.1. Section Sizes

One equal angle section size, L50×50×2.5, was tested, having a nominal leg length of 50 mm and a nominal thickness of 2.4 mm. This section size was selected since it was the most slender section used in the previous test program reported in Popovic et al. (1999). The angles tested in this report were produced on the same mill as those reported in Popovic et al. (1999). The nominal and measured dimensions of all test specimens are presented in Table 1, except for the measured leg length which was the same as the nominal value within the accuracy of measurement, ie 50 mm.

The section slenderness is expressed in terms of the ratio of the effective area calculated at the yield stress to the gross area, also referred to as the form factor (k_f). According to AS 4100, the value of the form factor (k_f) was 0.602, based on nominal values of thickness and yield stress of 2.4 mm and 400 MPa respectively.

2.2. Tensile Coupon Tests

2.2.1. Procedure

Tensile coupons were prepared and tested according to the Australian Standard "Methods for Tensile Testing of Metals" AS 1391-1991 to determine the yield stress (f_y), tensile strength (f_u), initial Young's Modulus (E) and percentage elongation after fracture (e_u). All coupons were tested in a 250 kN capacity Instron universal testing machine using friction grips to apply loading.

During the cold-forming process, a section is formed from an initially flat strip of steel on coil which has nearly uniform material properties in the direction of rolling. The sheet is passed through various sets of rollers and gradually brought into the desired shape. Each set of rollers inputs some amount of cold work causing additional residual strain in the section. The distribution of the residual strain varies along the width of the section since different amounts of cold work are input at the tips, middle of the leg and the corner. The amounts of strain input due to the forming process affects the shape of the stress-strain curve, the value of the yield stress and the percentage elongation of the material.

To determine the variation of material properties due to cold-forming, six coupons were taken from the positions shown in Figure 2 across the width of the flat portion of the leg and one coupon was taken from the corner. The coupon positions coincided with the position of the strips cut to measure the residual strains, as described in Popovic et al. (1996). The coupons were cut so that their longitudinal axis was parallel to the direction of roll-forming. No straightening was applied to the coupons, and the surface finish was as-manufactured. The initial cross-sectional area of the coupons cut from the flats was calculated as the product of the measured width and thickness of the parallel length of the coupon. Since the shape of the corner coupon was non-rectangular, the cross-sectional area was determined by weighing the parallel length, which was initially 80 mm, after the test was performed.

Each tensile coupon was instrumented with two linear strain gauges before testing. A Spectra MS-208 data acquisition system was used to record the load and the strain gauge readings which were taken at regular time intervals (3-10 seconds) during the test. The coupons were tested using a strain rate of about 1.4×10^{-4} sec^{-1} in the elastic range and a strain rate of about 5.6×10^{-4} sec^{-1} in the plastic range. Static loads in the vicinity of yield and ultimate were recorded by stopping the test for one minute and recording the true static readings.

2.2.2. Test Results

The measured values of f_y, f_u, E and e_u are reported in Table 2 for the seven coupons tested. The stress-strain curves of the tensile coupons cut from the flat part of the section and the corner are shown in Figure 3, where the strain is the membrane strain determined as the mean of the two strain gauge readings and the stress is the measured load divided by the initial area. For the coupons cut from the middle of the flat, the lower yield stress is reported, since the stress-strain curves showed conventional yield behaviour with upper and lower yield points. The 0.2 % proof stress ($f_{0.2}$) is reported as the yield stress for the coupons cut in the vicinity of and at the corner and at the tip of the leg, since the material did not exhibit a yield plateau at these locations. Most of the cold work was induced at these locations and hence the proof stresses were generally higher than the yield stresses measured near the centre of the leg. The distributions of yield stress, tensile strength and percentage elongation after fracture along the leg width are shown in Figure 4. As expected, the material with tensile properties enhanced due to cold work has lower percentage elongations after fracture, i.e. it is less ductile. The curve in Figure 3, representing the tensile coupon of the corner, shows that the material with the highest amount of cold work fractures at much lower elongation than the material from the rest of the section. The measured static value of the yield

(proof) stress varied from 415 MPa at the middle of the leg to 568 MPa at the corner.

Coupons were also cut from the middle of four different flats of the same section size. The average measured value of the static yield stress was 401 MPa and this value has been used to generate the design curves in later sections of this report.

2.3. Residual Strain

The results of the residual strain measurement, reported in detail in Popovic et al. (1999), are used in this report. This is deemed acceptable because the angles used for the present investigation were produced on the same roll-forming mill as those tested in Popovic et al (1999). The measurements reported in Popovic et al. (1999) are summarised as follows: The residual strain was measured using a Cambridge Insitu Extensometer (Denston and White, 1977). The results of the membrane strain measurements are reproduced in Table 3. The distribution of the residual membrane strain along the cross section width is shown in Figure 5 where the numbers on the horizontal axis correspond to the locations shown in Figure 2. The test results show that a compressive strain was located at the tip of the legs and at the corner while the mid-part of the flats was strained in membrane tension. The maximum compressive membrane strain was at the corner of the section and was as high as 1200 μstrain, which is equivalent to a stress of 240 MPa. The maximum tensile membrane strain was about 500 μstrain, corresponding to 100 MPa.

Comparing Figures 4 and 5, a direct correlation can be drawn between the yield stress and the compressive residual membrane strain. Higher residual stress is associated with higher yield (proof) stress. The opposite correlation applies to the relationship between the percentage elongation after fracture and the compressive residual membrane strain.

3. Compression Tests

3.1. Stub Column Tests

The results of the stub column tests are reported in detail in Popovic et al. (1999). No additional stub column testing was conducted for the present test series. The stub column tests were performed in accordance with Appendix B of Galambos (1988). The purpose of the tests was to determine the average stress-strain relationship for the complete cross section and the section compressive strength (N_s).

Two specimens were tested at a length of 150 mm. The average value of the measured static compressive strength of the section was 71.4 kN which

corresponded to a stress of 320 MPa. The failure of both stub column samples occurred by inelastic local buckling of the legs. The average stub column strength of 71.4 kN can be assumed to be an accurate lower bound for the angles tested in this report, since the measured yield stress at the centre of the flat of the stub columns was 388 MPa (Popovic et al. 1999) which was slightly lower than the value of 401 MPa determined for the present test specimens.

3.2. Long Columns Loaded Parallel with a Leg

3.2.1. Test Rig

A schematic diagram of the test rig is shown in Figures 6 and 7, and a long column specimen under test is shown in Figure 8. The test rig consisted of two main independent components, a reaction frame and a measurement frame.

A 250 kN servo-controlled hydraulic actuator was used to apply compressive axial force to the specimen, as shown in Figure 6. A moveable end support allowed tests to be conducted at specimen lengths of up to four metres.

The lateral deflection perpendicular to the loaded leg and twist-rotation at the mid-span of the specimen were obtained by using the measurement frame shown in Figures 7 and 8. The frame supported three linear transducers which measured the movement of a local frame that followed the deformation of the specimen during overall flexure and torsion. The local frame was built from aluminium and supported using counter-weights so as not to apply lateral loads to the specimen. The transducers were connected to a data logger acquisition system interfacing with a PC.

Separate transducers were used to measure the movement of the end bearing attached to the hydraulic jack. The measurement has been corrected for the flexibility of the frame supporting the other end bearing to give the shortening of the specimen.

The pin-ended bearings were designed to allow rotations about an axis parallel with one leg, while rotations about the perpendicular axis and twist rotations were restrained, as shown in Figure 9. Each bearing consisted of a thick steel plate mounted on a shaft allowing rotation about the vertical axis. The specimens had 20 mm thick rectangular steel plate welded to each end. The plates had bolt holes at the corners allowing the specimen to be bolted to the bearings. The specimens were positioned so that one leg was parallel with the axis of the support rotation.

3.2.2. Sample Designation

The format of the specimen designation is,

PL24 *l n*

where *l* represents the loading position (L - through the centre of the leg, C - through the centroid of the section and O - outside the section) and *n* is an integer representing the length such that lower numbers imply shorter lengths. The designations and actual lengths of the test samples are given in Table 4.

3.2.3. Initial Imperfections (out-of-straightness)

The initial imperfections were measured for all specimens except PL24L4 and PL24L5. A theodolite with micrometer plates was used for the measurement. The imperfections were measured at the tips of the legs in the plane perpendicular to the leg, and at the corner in the plane of the major principal axis. The maximum measured imperfections for each test specimen are presented in Table 4. The table shows the imperfections of the tips of the legs and of the corner, as well as the twist rotation of the section. The positive directions of the measurements are shown in Figure 10. A positive sign corresponds to an imperfection towards the inside of the section. The measurements were taken at every 50 mm or 100 mm depending on the specimen length. The specimens experienced much higher imperfections at the tips of the legs than at the corner since twist rotation was included. The maximum measured imperfection of the tips of the legs was L/604 for specimen PL24L1, and of the corner L/1092 for specimen PL24O1, where *L* is the actual length of the specimen. The average measured imperfections for all test specimens were L/1168 for the tips of the legs and L/2955 for the corner.

3.2.4. Long Column Tests

A total of eleven L50x50x2.5 specimens were tested; five of them were loaded through the centre of the leg (PL24L tests), three through the centroid of the section (PL24C tests) and three through a point outside the section at a distance from the centre of the leg equal to the distance between the centre of the leg and the centroid of the section (PL24O tests). The specimens were aligned such that the vertical leg of the specimen was parallel with the axis of the rotation of the support, forcing the specimen to bend at the ends in the horizontal non-principal plane. The load was applied continuously under stroke control of the axial hydraulic actuator at a very low rate (approximately 0.005 mm/sec), so that the measurements could be assumed to be static.

The test results are presented in Table 5 as the specimen length, effective length and ultimate load (strength) for each specimen. The test strengths are also presented in graphical form in Figures 11 and 12. The property on the horizontal axis is the slenderness of the section expressed as L_e/r_h where L_e is the effective length and r_h is the radius of gyration about the non-principal axis parallel with the leg. The distance between the ends of the specimen and the axes of rotation was 96 mm at both supports. Thus the effective length (L_e) was

taken as: $L_e = f\times(L + 2\times 96$ mm), where L is the actual specimen length and f is a factor that accounts for the increase in the elastic overall buckling load caused by the enhanced stiffness of the end bearings. The effective lengths (L_e) are presented in column 3 of Table 5. The lowest value of f was about 0.95 leading to shorter effective lengths for very short specimens. The factor (f) was virtually unity for longer specimens.

The curves of load versus lateral deflection perpendicular to the loaded leg at mid-span for each specimen are shown in Appendix C, the curves of load versus twist rotation at mid-span are shown in Appendix D and the curves of load versus rotation of the end bearings are shown in Appendix E.

The test specimens failed in local, torsional, flexural or flexural-torsional modes, depending on the effective length and the loading eccentricity. The failure modes were deduced from the inelastic deformations observed at the conclusion of the tests. The shortest specimens PL24C1, PL24L1 and PL24O1 (length no. 1) failed in local or torsional modes, as shown in Figure 13. Specimens PL24L1 and PL24O1 suffered local buckling of the vertical leg (parallel to the axis of bending) since the loading produced higher compressive stress in this leg than in the horizontal leg. The PL24C1 specimen suffered torsional buckling with twisting of both legs, although the horizontal leg suffered larger localised deformations eventually. Specimens PL24C2 and PL24L2 (length no. 2) failed in a flexural-torsional mode, as shown in Figure 14, while specimen PL24O2 and the rest of the longer specimens (lengths no. 3 to 5) failed in flexural modes. The failure mode of each specimen is shown in Figures 11 and 12.

The lateral deflection at mid-span perpendicular to the axis of bending increased with increasing specimen length, exceeding $L_e/50$ in some cases at the ultimate load. Prior to the ultimate load, the sections experienced a very high twist at the mid-span (see Figure 8) which was associated with a deflection approximately in the direction of the major principal axis. However, there was no apparent permanent twist deformation or local buckling of the legs after the tests, as shown in Figure 15. The post-ultimate behaviour was generally ductile without a sudden drop in load for the longer specimens.

The PL24C and PL24O specimens were tested to investigate the sensitivity to the position of the loading compared to loading through the leg (PL24L specimens). The test results show that the strengths are sensitive to the direction of the eccentricity especially for shorter specimens. Loading points closer to the centroid of the section increase the column capacity and extend the length range associated with failure in a flexural-torsional mode. The opposite orientation of the load makes the flexural failure mode more dominant and reduces the ultimate load of the column. As an example, specimens PL24O1

and PL24C1 failed at loads which were 27 % lower and 29 % higher than specimen PL24L1 respectively.

4. Design Rules

4.1. AS 4100-1998

AS 4100 has special provisions for eccentrically loaded double-bolted or welded single angles in trusses, as specified in Clause 8.4.6 of the standard (Standards Australia 1998). The following requirements shall be satisfied:

$$\frac{N^*}{N_{ch}} + \frac{M_h^*}{M_{bx}\cos\alpha} \le 1.0 \qquad (1)$$

$$\frac{N^*}{N_s} + \frac{M_x^*}{M_{sx}} + \frac{M_y^*}{M_{sy}} \le 1.0 \qquad (2)$$

where N^* is the design axial force in the member, N_{ch} is the nominal member capacity in axial compression of a single angle compression member buckling about the h-axis parallel with the loaded leg, N_s is the nominal section axial compression capacity, M_h^* is the design bending moment acting about the h-axis parallel with the loaded leg, M_x^* and M_y^* are the design bending moments acting about the major x- and minor y-axis, respectively, M_{bx} is the nominal member moment capacity for an angle in uniform bending without full lateral support, bent about the major principal x-axis, M_{sx} and M_{sy} are the nominal section moment capacities about the x- and y-axis, respectively, and α is the angle between the h-axis and the major principal x-axis ($\alpha = 45°$ in this investigation). For shorter members where $L/t \le 35\ (250/f_y)$, M_{bx} may be taken as M_{sx}.

The design bending moment (M_h^*) includes the second order moment resulting from the compressive loads acting on the member in its deformed configuration.

The moments (M_{he}^*) acting at the *ends* are equal to $N^* \times e$ where the eccentricity ($e = c_h - t/2$) is with respect to the geometric centroid, as shown in Figure 1. In the figure, c_h is the perpendicular distance from the outside face of the loaded leg to the centroid. The design bending moment (M_h^*) is taken as the maximum bending moment in the member. For a member in uniform bending, the maximum bending moment occurs at the centre and is (Trahair and Bradford, 1988):

$$M_h^* = \delta_b M_{he}^* \qquad (3)$$

$$\delta_b = \sqrt{1 + \left(\beta \csc\left(\pi \sqrt{\frac{N^*}{N_E}} \right) + \cot\left(\pi \sqrt{\frac{N^*}{N_E}} \right) \right)^2} \qquad (4)$$

where M_{he}^* is the end bending moment equal to $N^* \times e$, δ_b is the moment amplification factor, β is the end moment ratio and is equal to -1.0 for the uniform bending moment distribution as in the present investigation, and N_E is the elastic buckling load with respect to the axis of bending, ie the *h*-axis parallel with the loaded leg.

4.2. AS/NZS 4600-1996 and AISI-1997

AS/NZS 4600 and the AISI Specification use the same design equations for angles. Unlike AS 4100, AS/NZS 4600 and the AISI Specification assume that the design actions are obtained from a first order analysis and the bending moment amplification factors are incorporated into the design equation. AS/NZS 4600 and the AISI Specification do not have special provisions for single angles loaded through one leg. This load case is treated as a combined axial compressive load and biaxial bending. The following requirements shall be satisfied:

$$\frac{N^*}{N_c} + \frac{C_{mx} M_x^*}{M_{bx} \alpha_{nx}} + \frac{C_{my} M_y^*}{M_{by} \alpha_{ny}} \le 1.0 \qquad (5)$$

$$\frac{N^*}{N_s} + \frac{M_x^*}{M_{bx}} + \frac{M_y^*}{M_{by}} \le 1.0 \qquad (6)$$

where N_c is the compressive member capacity based on the least of the elastic minor principal axis flexural buckling stress and the flexural-torsional buckling stress, N_s is the compressive section capacity, and M_x^* and M_y^* are the design bending moments calculated as the projections of the bending moment M_h^* onto the principal *x*- and *y*-axes respectively, i.e.

$$M_x^* = M_h^* \cos\alpha \qquad (7)$$

$$M_y^* = M_h^* \sin\alpha \qquad (8)$$

where α is the angle between the *h*-axis parallel to the loaded leg and the major principal *x*-axis, assuming the sign convention shown in Figure 1. In Equation (5), M_{bx} and M_{by} are the member capacities for bending about the principal *x*- and *y*-axes, respectively, C_{mx} and C_{my} are coefficients accounting for unequal end moment, and α_{nx} and α_{ny} are moment amplification factors.

For short members where $N^*/N_c \le 0.15$ the following interaction equation can be used in lieu of Equations (5) and (6):

$$\frac{N^*}{N_c} + \frac{M_x^*}{M_{bx}} + \frac{M_y^*}{M_{by}} \le 1.0 \qquad (9)$$

4.3. ASCE-1991

In the American Society of Civil Engineers (1991) Standard for Design of Latticed Steel Transmission Structures, the design capacity ($N^* = F_a \times A_g$) of axially loaded compression members is given as the product of the gross cross-sectional area and compression stress F_a, calculated as

$$F_a = \left[1 - \frac{1}{2}\left(\frac{KL/r}{C_c}\right)^2\right] F_{cr} \qquad for \quad \frac{KL}{r} \le C_c \qquad (10)$$

$$F_a = \frac{\pi^2 E}{\left(\frac{KL}{r}\right)^2} \qquad for \quad \frac{KL}{r} \ge C_c \qquad (11)$$

$$C_c = \pi\sqrt{\frac{2E}{F_{cr}}} \qquad (12)$$

where F_{cr} is the critical stress for local buckling, C_c is the column slenderness ratio separating elastic and inelastic buckling, KL is the effective length and r is the radius of gyration about the minor principal axis.

For the width-to-thickness ratio (w/t = 19.31) of the L50x50x2.5 section, the corresponding F_{cr} is:

$$F_{cr} = \frac{0.0332\pi^2 E}{(w/t)^2} \qquad (13)$$

where w is the flat width of the leg outside the corner region.

The ASCE Standard provides formulae for the effective slenderness ratio (KL/r) which account for the effects of end restraint and loading eccentricity in transmission structures where diagonal angle members are connected to flexible leg members through one leg. The KL/r-formulae are adjusted such that loading eccentricity is the dominant factor in the lower KL/r-range while rotational restraint is the dominant factor in the higher KL/r-range. In the present investigation, the members were subject to loading eccentricities but

unrestrained rotationally at the ends. Consequently, the appropriate formulae for *KL/r* are,

$$\frac{KL}{r} = 60 + 0.5\frac{L}{r} \qquad for \quad 0 \le \frac{L}{r} \le 120 \tag{14}$$

$$\frac{KL}{r} = \frac{L}{r} \qquad for \quad 120 \le \frac{L}{r} \le 200 \tag{15}$$

4.4. AISC-1993

In the American Institute of Steel Construction (1993) Specification for Load and Resistance Factor Design of Single-Angle Members, the design rules for combined compression and bending given in Clause 6.1 allow section moduli for specific locations in the cross-section and distinction between compressive and tensile stresses to be taken into account. For angles loaded at the connected leg, this leads to checking yielding in compression at the connected leg,

$$\frac{P_u}{2P_n} + \frac{M_u B_1}{M_{nc}} \le 1 \quad for \quad \frac{P_u}{P_n} \le 0.2 \tag{16}$$

$$\frac{P_u}{P_n} + \frac{8}{9}\frac{M_u B_1}{M_{nc}} \le 1 \quad for \quad \frac{P_u}{P_n} \ge 0.2 \tag{17}$$

and yielding in tension or compression at the tip of the unconnected leg,

$$\left|\frac{P_u}{2P_n} - \frac{M_u}{M_{nt}}\right| \le 1 \quad for \quad \frac{P_u}{P_n} \le 0.2 \tag{18}$$

$$\left|\frac{P_u}{P_n} - \frac{8}{9}\frac{M_u}{M_{nt}}\right| \le 1 \quad for \quad \frac{P_u}{P_n} \ge 0.2 \tag{19}$$

The following comments apply to Equations 16-19:

- The design actions (P_u, M_u) and resistances (P_n, M_n) are taken as positive,
- (M_u) is the design bending moment about the loaded leg, calculated as $P_u \times e$ where $e = c_h - t/2$ is the distance from the centroid to the centre-line of the loaded leg,
- $M_{nt} = S_{ht} F_y$ is the nominal flexural strength for bending about an axis parallel to the loaded leg leading to yielding at the tip of the unconnected leg,

- M_{nc} is the nominal flexural-torsional buckling strength for bending about an axis parallel to the loaded leg, determined according to Clauses 5.1.1, 5.1.3 and 5.2.2 using S_{hc} to determine M_y,
- B_1 is the moment amplification factor computed as $1/(1-P_u/P_{e1})$ where P_{e1} is the Euler load based on a radius of gyration of $r_h/1.35$ where r_h is the radius of gyration of an axis parallel to the loaded leg, as set out in Clause 6.1.3, and
- P_n is the column strength computed in accordance with Clause 4.

In computing the design compressive strength, $P_n = A_g F_{cr}$, A_g is the gross cross-sectional area and,

$$F_{cr} = Q\left(0.658^{Q\lambda^2}\right)F_y \qquad for \quad \lambda_c\sqrt{Q} \le 1.5 \tag{20}$$

$$F_{cr} = \left[\frac{0.877}{\lambda_c{}^2}\right]F_y \qquad for \quad \lambda_c\sqrt{Q} \ge 1.5 \tag{21}$$

where F_y is the nominal yield stress and

$$\lambda_c = \frac{KL}{r\pi}\sqrt{\frac{F_y}{E}} \tag{22}$$

Since for the present test series,

$$\left(\frac{b}{t} = 21.46\right) \ge \left(0.910\sqrt{\frac{E}{F_y}} = 20.32\right) \tag{23}$$

the reduction factor for local buckling Q is:

$$Q = \frac{0.534E}{F_y\left(\frac{b}{t}\right)^2} \tag{24}$$

where b is the full length of angle leg (50 mm in this case). It is not specified whether the radius of gyration (r in Equation 22) shall be with respect to the minor principal axis or an axis parallel to the loaded leg. Strength curves using both radii of gyration are considered in this report.

The AISC Specification only requires amplification of the moment when checking yielding where the moment induces compression. Accordingly, the B_1 factor is only included in Equations 16-17 and not in Equations 18-19. The reason for this distinction is probably that axial force (P_u) is likely to be small when the M_u/M_{nt}-term of Equations 18-19 is the governing term so that the

effect of moment amplification is insignificant. When the P_u/P_n-term of Equations 18-19 governs, it is conservative to ignore moment amplification. For the angle section considered in this report, compression yielding at the loaded leg (Equations 16-17) always governed.

5. Comparison of Test Results with Design Standards

5.1. Comparison with AS 4100, AS/NZS 4600, ASCE and AISC

The test strengths are compared with design strength curves in Figure 11. The radius of gyration used to nondimensionalise the effective length is calculated with respect to an axis parallel with the loaded leg. The design strengths were calculated using the mean measured value of yield stress of the legs of f_y = 401 MPa and mean measured cross-section dimensions, as shown in Table 1. The design curves were computed assuming loading through the centre-line of the connected leg, and so shall be compared with the PL24L tests.

It appears from Figure 11 that the AS 4100 strength curve is conservative especially for the shorter specimens. For the specimen with a slenderness value of L_e/r_h = 28.7, the test strength is more than twice the design strength, as also shown in Table 5. As the length increases, the design strengths slowly approach the test strengths. However, for the longest specimen tested (L_e/r = 142.6), the test strength is still 41 % above the design value.

The AS/NZS 4600 and AISI design curve appears to be even more conservative than the AS 4100 curve. The test strengths are between 109 and 186 % higher than the values predicted by the standards, as shown in Table 5. The conservatism stems partly from the assumption that the case of a compression angle bent about a leg is to be treated as an angle in combined axial compression and principal axis bending, although the specimen is forced to bend about a non-principal axis at the ends. As a result of this assumption, the nominal member capacity in compression N_c is calculated using the critical buckling stress based on the least of the elastic minor principal axis flexural buckling stress and the flexural-torsional buckling stress. In AS 4100, the nominal member capacity in compression N_{ch} is based on the critical load for flexural buckling about the non-principal *h*-axis parallel with the loaded leg and is much higher than the corresponding value of N_c of AS/NZS 4600 and the AISI Specification. Within the slenderness range of $0 \le L_e/r_h \le 200$, the ratio N_{ch}/N_c is between 1.23 and 2.5. The largest difference between the two nominal member capacities in compression is for very short and very long specimens. The smallest difference is for a slenderness L_e/r_h of about 60 where the governing failure mode in AS/NZS 4600 and the AISI Specification, switches from flexural-torsional to flexural as length is increased. For very short

specimens $N_{ch} = N_s$ according to AS 4100 whilst $N_c \sim 0.54\, N_s$ according to AS/NZS 4600 and the AISI Specification because flexural-torsional buckling implies a reduction factor of 0.54 for $L_e/r_h \to 0$. The substantial difference in the two nominal member capacities in compression is the main reason for the higher design capacities of AS 4100.

However, it is also significant that the interaction equations used in AS 4100, AS/NZS 4600 and the AISI Specification do not consider yielding at specific points in the cross-section, as is allowed in the AISC Specification. The bending capacities are based on yielding at the tip of the unloaded leg whereas the use of the AISC Specification showed that yielding occurs first in compression at the loaded leg so that the higher bending capacity associated with yielding at this leg should be used.

The ASCE Standard is in reasonable agreement with the tests, although conservative at short and long lengths. The design curve may be optimistic in the intermediate slenderness range ($L_e/r_h \sim 80$). However the test strength in this range (specimen PL24L3) appears to be low compared to the general trend of the PL24 test strengths.

The two curves shown for the AISC Specification are for compressive strengths (P_n) computed using the minor principal axis radius of gyration (r_y) and the radius of gyration (r_h) for bending about an axis parallel to the loaded leg. Both curves are conservative, particularly at short and intermediate lengths. The curve based on r_h is nearly indistinguishable from the AS 4100 strength curve at long lengths. The same applies to the AISC curve based on r_y and the AS 4600/AISI strength curve. Part of the reason for the low design strengths obtained using r_y is that the effective length is taken as the pin-ended length. When considering bending about the minor principal axis, the ends are somewhere between fixed and pinned and the effective length is actually shorter than the pin-ended length. This is a result of the fact that rotations about an axis parallel with the loaded leg are unrestrained whereas the perpendicular rotation is restrained. Higher design strengths would result if the actual effective length was used. However, this is not easily calculated.

5.2. Proposed Design Method in AS/NZS 4600

Although AS 4100 does not take into account the flexural-torsional mode as a possible mode of failure, it predicts more accurately the failure load of members loaded parallel with the leg. It can be seen from column 10 of Table 5 that, for the specimens tested, AS 4100 gives 20 % to 48 % higher capacities than AS/NZS 4600 and the AISI Specification. At the same time AS 4100 is still very conservative.

One possible way to improve the AS/NZS 4600 and AISI design method would be to exclude the flexural-torsional mode of buckling from the design procedure, as it is done in AS 4100. In this case, the least elastic buckling stress (f_{oc}) shall be calculated as the critical stress for flexural buckling about the minor principal axis, as specified in Clause 3.4.2 of AS/NZS 4600 and Clause C4.1 of the AISI Specification. The curve obtained using this proposal is shown in Figure 12. The maximum improvement of the design capacity for the L50x50x2.5 section is 30.8 % for very short specimens. The improvement is negligible for specimens with $L_e/r > 75$.

Ignoring the flexural-torsional buckling stress in computing the column strength does not imply that torsion is completely ignored in the design procedure, since local buckling is considered in determining the effective area, and the local mode is identical to the torsional mode at vanishing lengths. By considering torsion in determining the effective area, the post-local buckling strength is accounted for. It is also important to note that torsion was not significant in the failure mode of the sections loaded through the leg at intermediate and long lengths.

It would appear that the design rule proposed in this section could be considered in the short term. However, the revised AS/NZS 4600 and AISI design curve is also very conservative compared to the test strengths. This suggests that in order to effectively improve the AS/NZS 4600 and AISI design procedures, it may be required to adopt a similar approach to that of the ASCE Standard (which empirically adjusts the effective length to produce agreement with tests).

6. Conclusions

The results of a series of compression tests on cold-formed in-line galvanised DuraGal L50x50x2.5 equal angles have been reported. The nominal thickness of the section was 2.4 mm so that the leg slenderness (b/t) was approximately 20, and the section could be regarded as fairly slender. A total of 11 specimens was tested under three conditions; loading through the centre of the leg (PL24L tests), loading through the centroid of the section (PL24C tests) and loading through a point outside the section at a distance from the centre of the leg equal to the distance between the centre of the leg and the centroid of the section (PL24O tests). In all cases, the specimen was forced to bend about an axis parallel with the loaded leg. The distribution of the stress-strain characteristics of the material and the residual strains have been reported, as have the initial imperfections.

The tests conducted using different loading eccentricity showed that compression angle members bent about an axis parallel with the leg are sensitive to the position of the load. If the loading point moves from the centre

of the leg closer to the section centroid, it increases the ultimate load and the flexural-torsional buckling mode becomes the dominant failure mode. If the loading point moves outside the section it reduces the column capacity and makes the flexural mode the dominant failure mode.

The comparisons of the test results with the design rules of AS 4100 (1998), AS/NZS 4600 (1996), the AISI Specification (1997), the ASCE (1991) Standard and the AISC (1993) Specification show that:

- The design capacities predicted by AS 4100, AS/NZS 4600 and the AISI Specification are very conservative compared with the test strengths, particularly those of AS/NZS 4600 and the AISI Specification. The conservatism is most pronounced for short specimens. The test strengths are 108 to 186 % higher than the predicted capacities according to AS/NZS 4600 and the AISI Specification. In the case of AS 4100, the test strengths are 41 % to 110 % higher.
- A slightly modified design method to be used in AS/NZS 4600 and the AISI Specification has been proposed. The method excludes the flexural-torsional buckling mode from the design procedure and considers only minor axis flexural buckling. It improves the design capacity by up to 30 % for the tested sections. However, the proposed method is still very conservative, suggesting that it may be required to completely redefine the design procedure for angles bent about a parallel leg, possibly along the lines of the ASCE Standard.
- The ASCE (1991) Standard is in reasonable agreement with the tests, although conservative at short and long lengths, and possibly optimistic at intermediate lengths.
- The AISC (1993) Specification is conservative, particularly at short and intermediate lengths. When the compression capacity is based on the radius of gyration about an axis parallel with the loaded leg, the Specification produces nearly the same strengths as AS 4100 at long lengths. When based on the minor axis radius of gyration, the Specification produces nearly the same strengths as AS/NZS 4600 and the AISI Specification at long lengths.

7. Acknowledgments

The authors are grateful to the Australian Research Council and BHP Structural and Pipeline Products for their support through an ARC Collaborative Research Grant. The experiments were carried out at the J. W. Roderick Laboratory for Materials and Structures of the Department of Civil Engineering at the University of Sydney.

8. Tables

Specimen	Thickness Including Coating t_c (mm)	Thickness of Bare Metal t (mm)	Outer Corner Radius r_o (mm)	Inner Corner Radius r_i (mm)	Radius of Gyration r_h^* (mm)	Yield Stress at Mid Leg f_y (MPa)	Length L (mm)
(1)	(2)	(3)	(4)	(5)	(6)	(7)	(8)
Nominal	**2.43**	**2.40**	**4.90**	**2.50**	**15.8**	**350**	
PL24C1	2.37	2.33	5.10	2.73	15.8	401	285
PL24C2	2.37	2.33	5.10	2.73	15.8	401	673
PL24C3	2.34	2.30	5.10	2.76	15.8	401	1100
PL24L1	2.34	2.30	5.10	2.76	15.8	401	284
PL24L2	2.34	2.30	5.10	2.76	15.8	401	665
PL24L3	2.34	2.30	5.10	2.76	15.8	401	1100
PL24L4	2.45	2.41	5.00	2.55	15.8	401	1580
PL24L5	2.45	2.41	5.00	2.55	15.8	401	2065
PL24O1	2.34	2.30	5.10	2.76	15.8	401	284
PL24O2	2.34	2.30	5.10	2.76	15.8	401	674
PL24O3	2.34	2.30	5.10	2.76	15.8	401	1100
Average Measured	**2.37**	**2.33**	**5.08**	**2.72**	**15.8**	**401**	

* r_h is the radius of gyration for bending about an axis parallel to the loaded leg.

Table 1: Specimen dimensions

Strip (1)	$f_{y\ static}$ (MPa) (2)	f_y (MPa) (3)	$f_{u\ static}$ (MPa) (4)	f_u (MPa) (5)	E (MPa) (6)	e_u (%) (7)
L1 (tip)	470	485	529	555	208977	18%
L2	442	457	506	532	210781	23%
L3	415	430	493	519	208742	24%
L4	417	432	497	523	208187	21%
L5	457	472	523	549	210836	16%
L6	477	492	546	572	208735	12%
L7 (corner)	568	583	618	638	200516	10%

Table 2: Tensile coupon test results

Initial ambient temperature: 24 ^{o}C

Ambient temperature after cutting: 23 ^{o}C

Strip	Reading				Surface Strain		Membrane strain	Membrane stress	Bending strain
	Before Cutting		After Cutting						
	Inner (mm)	Outer (mm)	Inner (mm)	Outer (mm)	Inner (μstrain)	Outer (μstrain)	(μstrain)	(MPa)	(μstrain)
(1)	(2)	(3)	(4)	(5)	(6)	(7)	(8)	(9)	(10)
1	-0.135	-0.268	-0.109	-0.273	-531	89	-221	-44	310
2	-0.348	-0.033	-0.337	-0.016	-231	-351	-291	-58	-60
3	-0.057	-0.110	-0.054	-0.116	-71	109	19	4	90
4	-0.205	0.014	-0.203	-0.015	-51	569	259	52	310
5	-0.223	-0.032	-0.221	-0.070	-51	749	349	70	400
6	0.011	-0.123	-0.014	-0.098	489	-511	-11	-2	-500
7	-0.164	-0.240	-0.142	-0.141	-451	-1991	-1221	-244	-770
8	0.153	-0.247	0.154	-0.257	-31	189	79	16	110
9	0.227	-0.053	0.229	-0.103	-51	989	469	94	520
10	0.000	0.014	0.006	-0.026	-131	789	329	66	460
11	0.094	0.043	0.103	0.018	-191	489	149	30	340
12	-0.056	-0.032	-0.046	-0.038	-211	109	-51	-10	160
13	0.138	-0.071	0.102	0.007	709	-1571	-431	-86	-1140

Table 3: Residual strain measurements, (Popovic et al. 1996)

Specimen	Length	Leg 1		Leg 2		Corner		Twist	
	(mm)	(mm)	(Δ_o/L)	(mm)	(Δ_o/L)	(mm)	(Δ_o/L)	(deg)	(deg/m)
(1)	(2)	(3)	(4)	(5)	(6)	(7)	(8)	(9)	(10)
PL24C1	285	0.33	L/874	0.40	L/714	0.19	L/1531	0.197	0.691
PL24C2	673	0.40	L/1683	0.80	L/841	0.16	L/4206	0.836	1.242
PL24C3	1100	1.13	L/973	0.39	L/2821	0.74	L/1486	1.489	1.354
PL24L1	284	0.47	L/604	0.35	L/811	0.09	L/3156	0.100	0.353
PL24L2	665	0.62	L/1073	0.76	L/875	0.19	L/3500	1.142	1.718
PL24L3	1100	0.81	L/1358	1.15	L/957	0.56	L/1964	1.135	1.032
PL24L4	1580	-	-	-	-	-	-	-	-
PL24L5	2065	-	-	-	-	-	-	-	-
PL24O1	284	0.46	L/617	0.32	L/888	0.26	L/1092	0.144	0.506
PL24O2	674	0.56	L/1204	0.56	L/1204	0.29	L/2324	1.353	2.007
PL24O3	1100	0.47	L/2340	0.93	L/1183	0.15	L/7333	1.081	0.982

Max Imperfection at the Tip	L/604
Mean Imperfection at the Tip	L/1168
Max Imperfection at the Corner	L/1092
Mean Imperfection at the Corner	L/2955

Table 4: Initial imperfections

Specimen	Specimen Length L (mm)	Effective Length L_e (mm)	Slenderness L_e/r_h*	Test Ultimate Load (kN)	Predicted Load (AS4100) (kN)	Predicted Load (AS4600/ AISI) (kN)	Predicted Load (ASCE) (kN)	Predicted Load (AISC**) (kN)	AS4100 / AS4600	Test / AS4100	Test / AS4600
(1)	(2)	(3)	(4)	(5)	(6)	(7)	(8)	(9)	(10)	(11)	(12)
PL24C1	285	455	28.8	56.88	-	-	-	-	-	-	-
PL24C2	673	857	54.2	46.57	-	-	-	-	-	-	-
PL24C3	1100	1287	81.4	33.57	-	-	-	-	-	-	-
PL24L1	284	454	28.7	44.09	21.04	15.44	33.24	22.71	1.36	2.10	2.86
PL24L2	665	849	53.7	34.56	16.88	13.95	29.95	17.82	1.21	2.05	2.48
PL24L3	1100	1287	81.4	22.37	12.89	10.77	24.17	12.23	1.20	1.74	2.08
PL24L4	1580	1768	111.9	15.90	9.60	7.07	13.52	7.72	1.36	1.66	2.25
PL24L5	2065	2253	142.6	10.25	7.27	4.90	8.33	5.23	1.48	1.41	2.09
PL24O1	284	454	28.7	31.99	-	-	-	-	-	-	-
PL24O2	674	858	54.3	25.90	-	-	-	-	-	-	-
PL24O3	1100	1287	81.4	17.14	-	-	-	-	-	-	-

* r_h is the radius of gyration for bending about an axis parallel to the loaded leg, r_h = 15.82 mm

** The AISC design loads are based on the minor axis radius of gyration for calculating P_n, r_y = 9.79 mm

Table 5: Test results

9. Figures

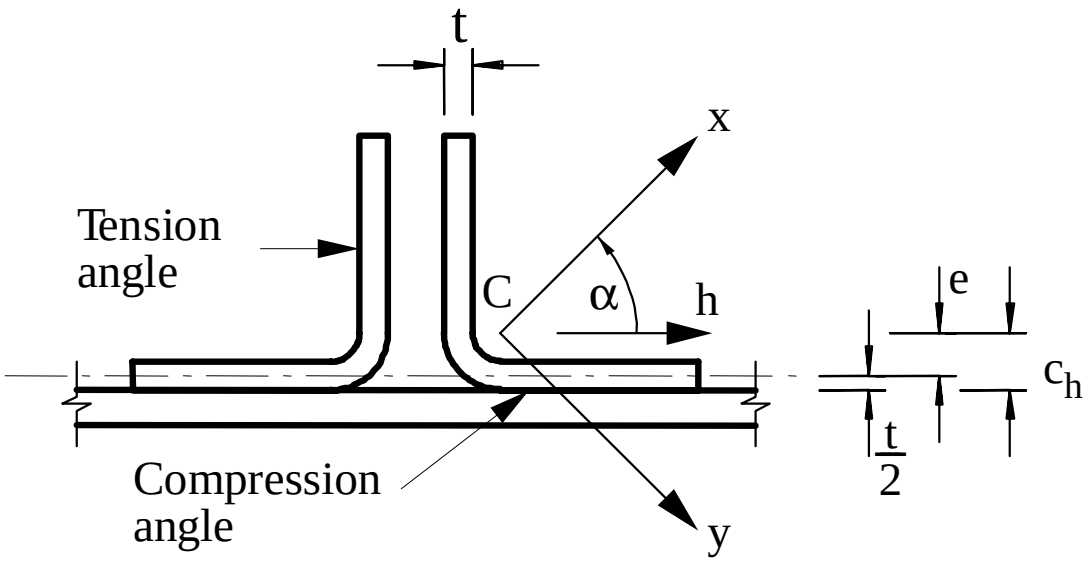

Figure 1: Eccentricity of angles on same side of chord

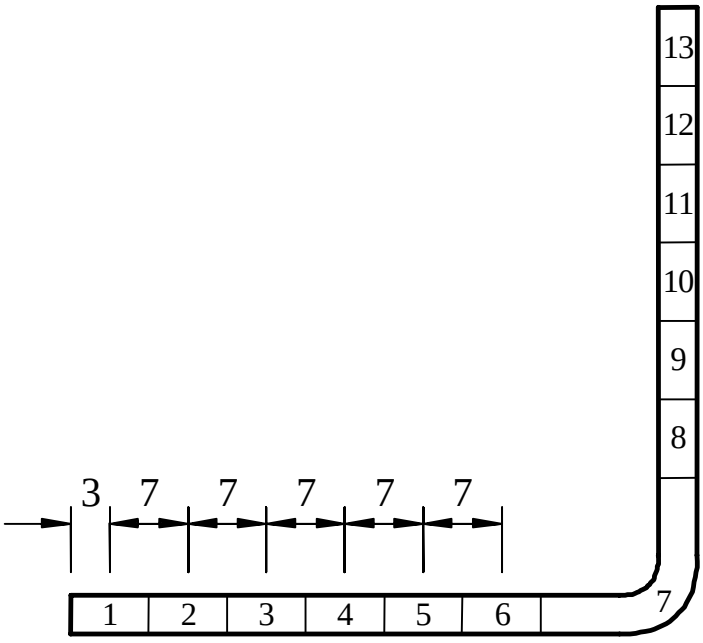

Figure 2: Positions of tensile and residual strain coupons

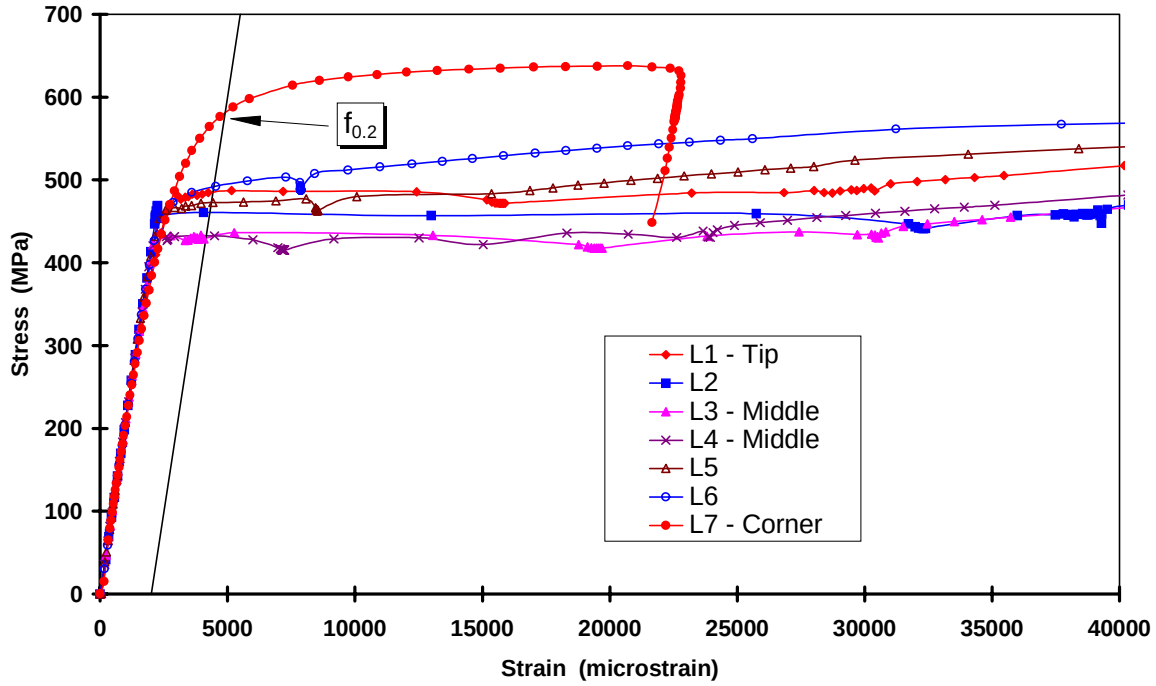

Figure 3: Stress-strain curves of coupons taken along a single leg

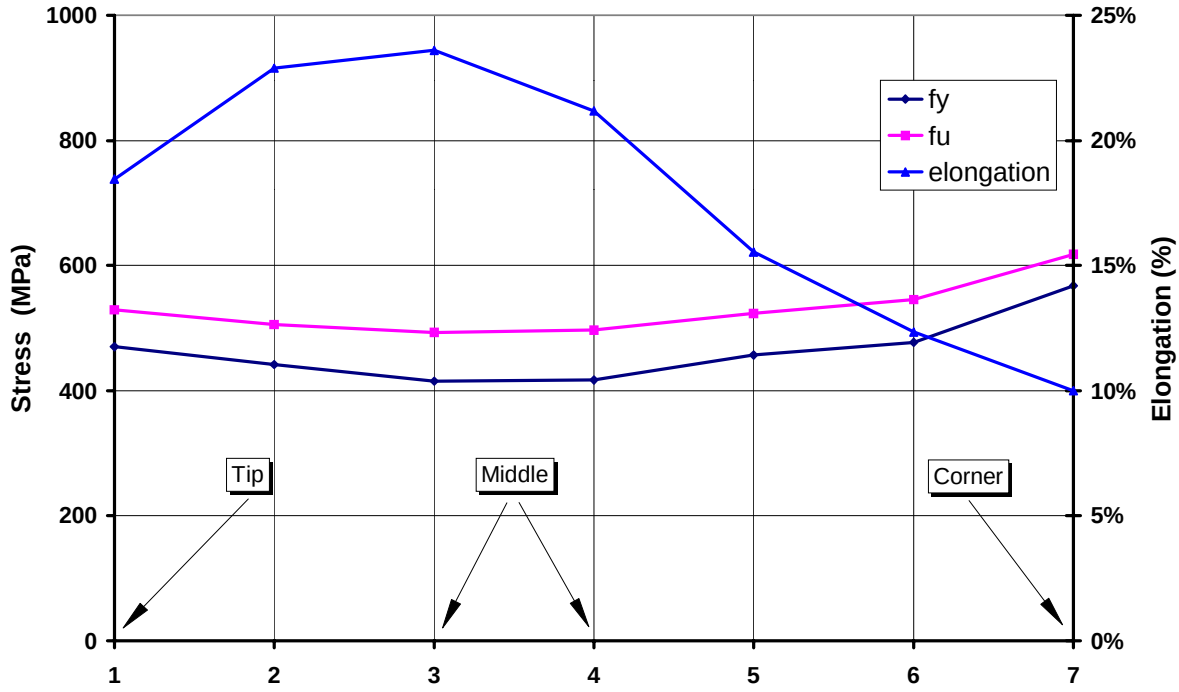

Figure 4: Stress and elongation distribution along leg width

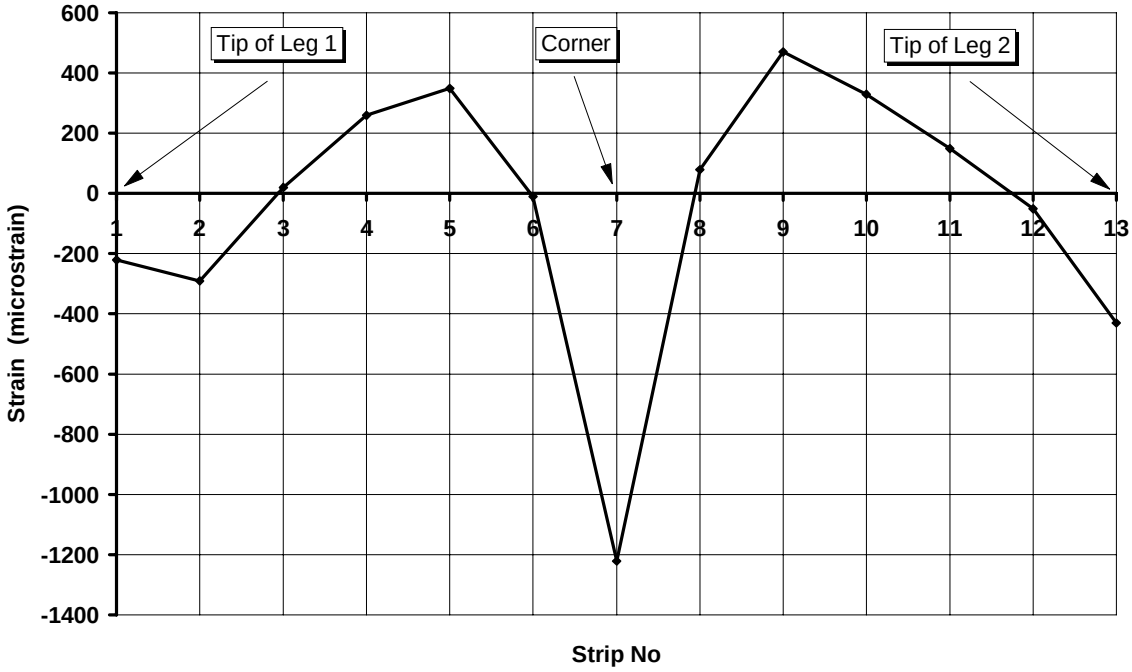

Figure 5: Residual membrane strain distribution along leg width, (Popovic et al. 1999)

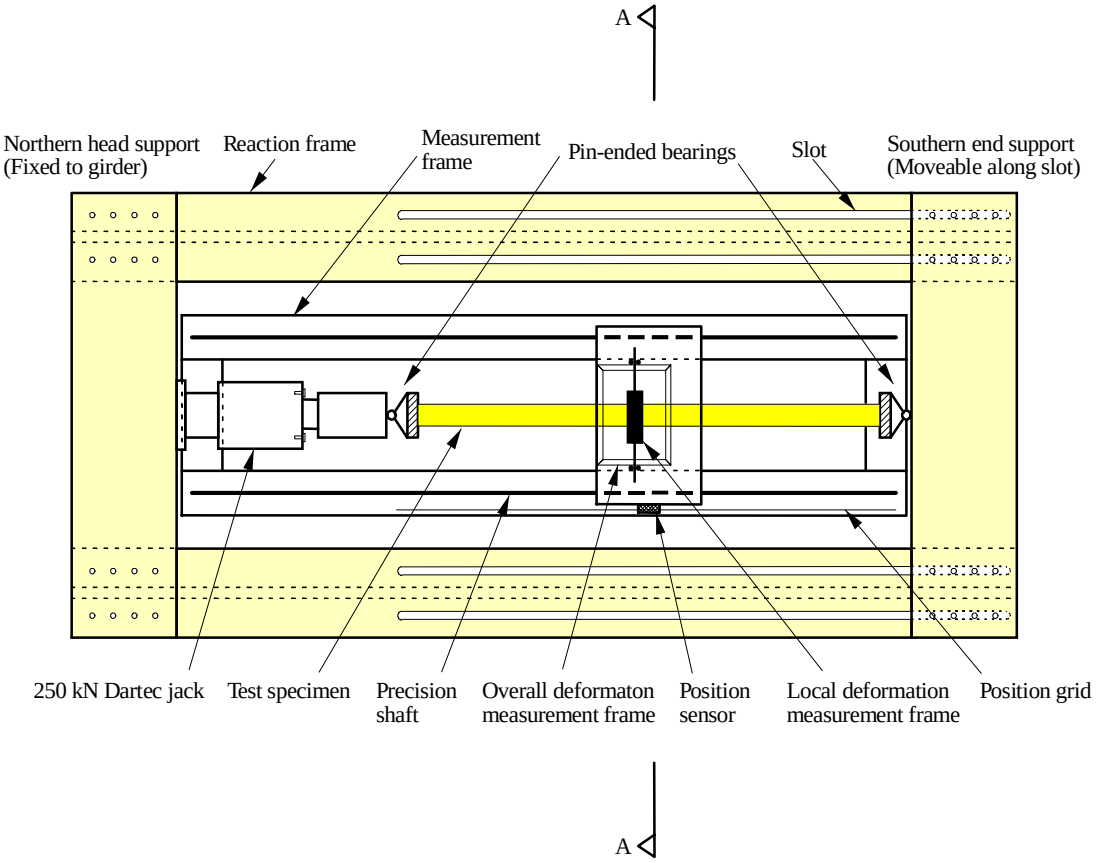

Figure 6: Long column test rig (schematic diagram)

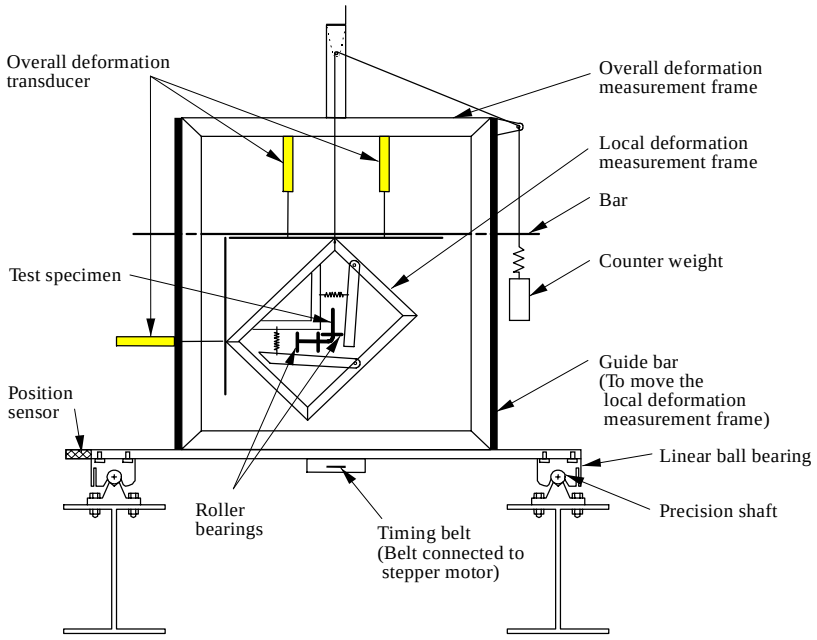

Section A-A

Figure 7: Measurement frames

Figure 8: Specimen under test (note twist at centre)

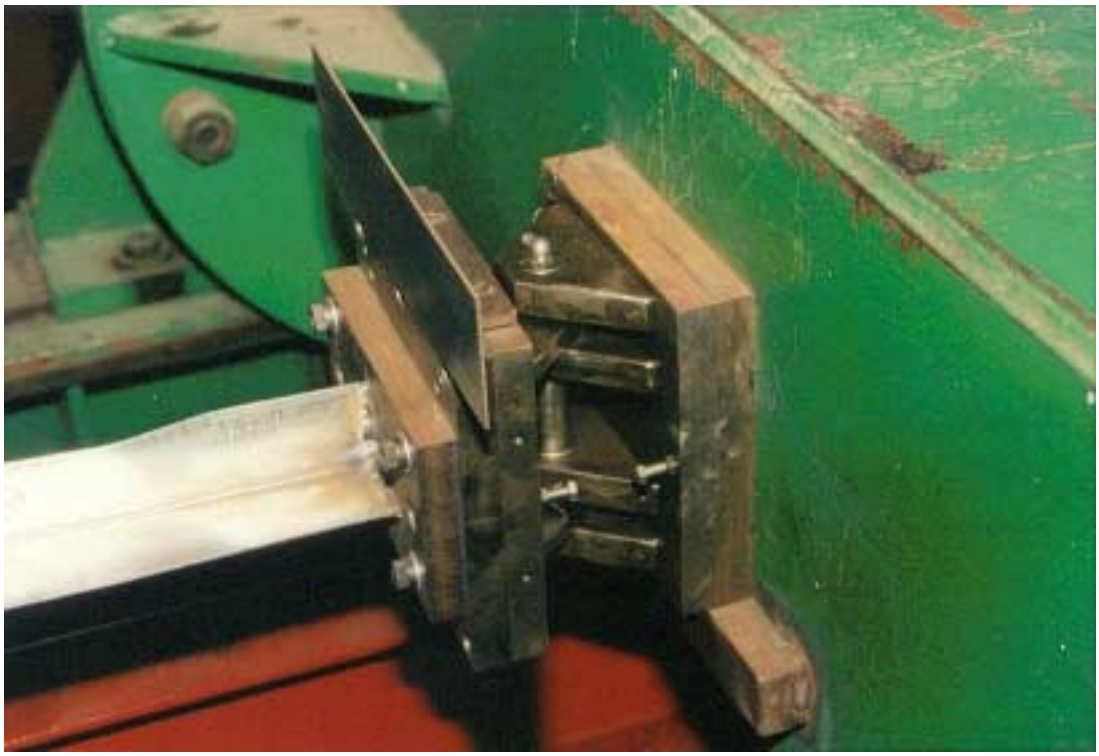

Figure 9: Pin-ended bearing

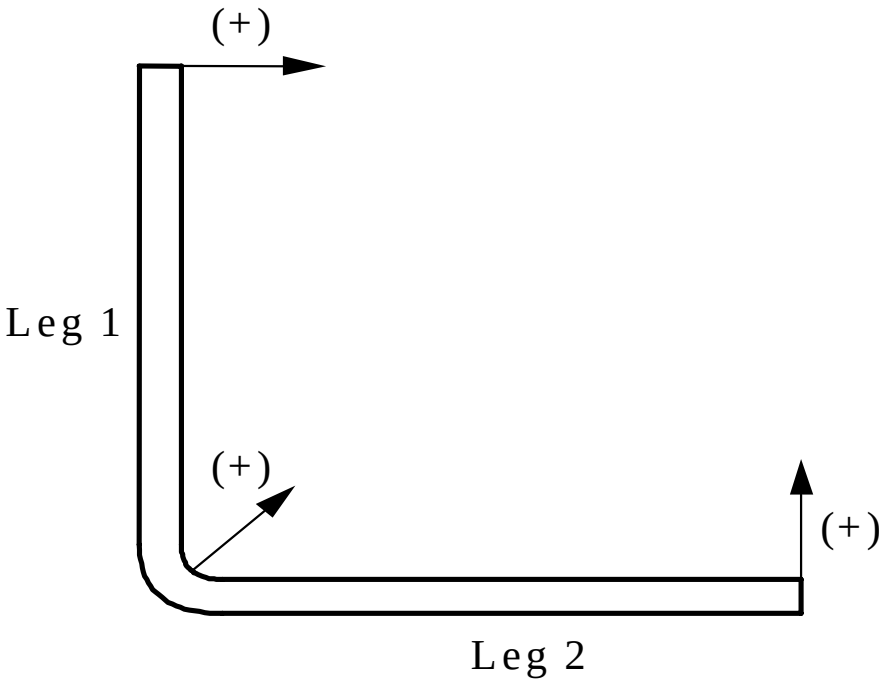

Figure 10: Directions of the measurements of initial imperfections

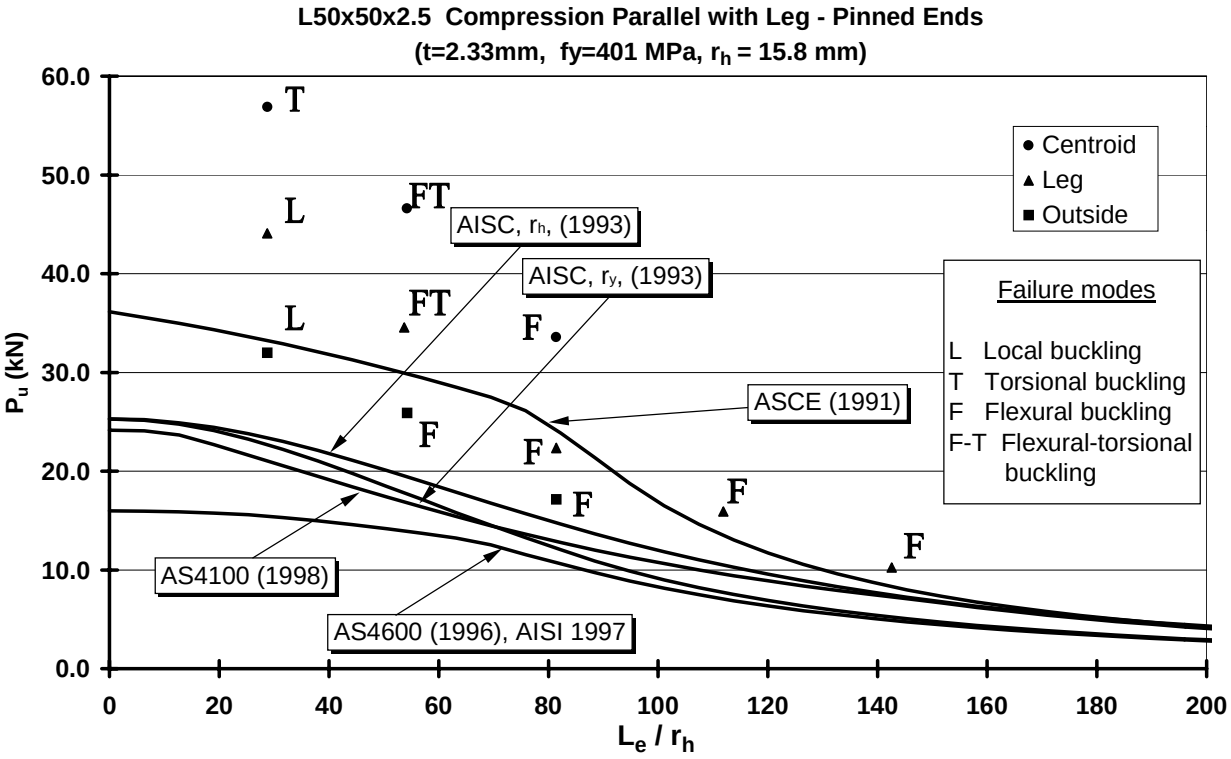

Figure 11: Test strengths vs design curves

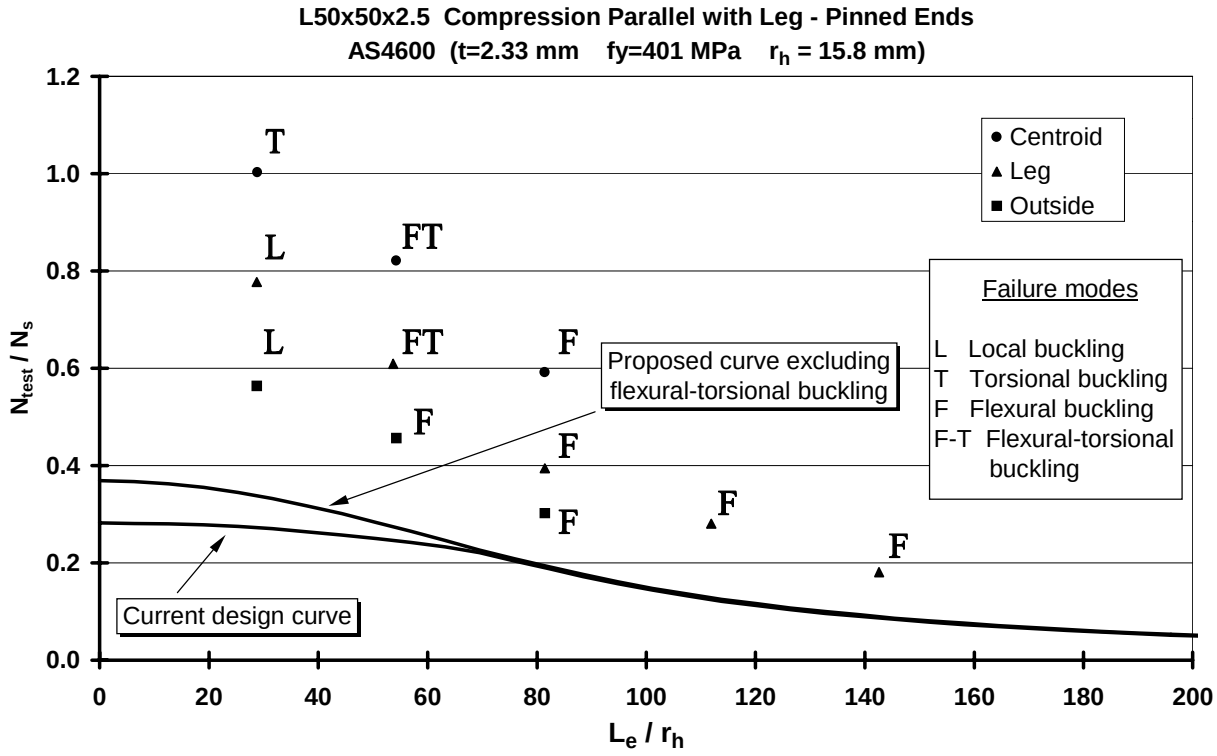

Figure 12: Test strengths vs AS/NZS 4600 and AISI design curves, (N_s=56.7 kN).

Figure 13: Failure of short specimens (Group 1)

Figure 14: Failure of specimens in Group 2

Figure 15: Failure of specimens of Group 3

APPENDICES

Appendix A. REFERENCES

American Institute of Steel Construction (1993), AISC, "Specification for Load and Resistance Factor Design of Single-Angle Members".

American Iron and Steel Institute (1997), AISI, Specification for the Design of Cold-formed Steel Structural Members, Washington DC.

American Society of Civil Engineers (1991), ASCE Standard, "Design of Latticed Steel Transmission Structures".

Denston, R. J. and White, J. D. (1977), "An Electrical Demountable Extensometer", Technical Report No CUED/C - Struct/TR.61, University of Cambridge, Department of Engineering.

Galambos, T. V. (1988), ed, *Guide to Stability Design Criteria for Metal Structures*, 4th Edition, John Wiley and Sons, New York.

Popovic, D., Hancock, G. J. and Rasmussen, K. J. R. (1996), "Axial Compression Tests of DuraGal Angles", Research Report No R730, Department of Civil Engineering, Centre for Advanced Structural Engineering, The University of Sydney, NSW, Australia.

Popovic, D., Hancock, G. J. and Rasmussen, K. J. R. (1999), "Axial Compression Tests of Cold-formed Angles", Journal of Structural Engineering, American Society of Civil Engineers, Vol . 125, No. 5, 515-523.

Standards Australia (1991), "Methods for Tensile Testing of Metals", Australian Standard AS 1391.

Standards Australia (1998), "Steel Structures", Australian Standard AS 4100.

Standards Australia / Standards New Zealand (1996), "Cold-Formed Steel Structures", AS/NZS 4600.

Trahair, N. S. and Bradford, M. A. (1988), *The Behaviour and Design of Steel Structures*, 2nd Edition, Chapman and Hall, New York.

Appendix B. NOTATION

Roman Letters

C_{mx}, C_{my} = Coefficients of unequal end moment (= 1.0 for uniform bending moment distribution)

c_h = Perpendicular distance to the centroid of the angle section from the face of the loaded leg of the angle

E = Young's modulus of elasticity

e = Eccentricity

e_h = Distance between the centroid and the outer edge of the leg

e_u = Percentage elongation after fracture

f_{oc} = Least of elastic buckling stresses

f_u = Ultimate tensile stress

f_y = Yield stress

k_f = Form factor for members subject to axial compression

L = Length of member

L_e = Effective length of member

M_{bx} = (AS4100) Nominal member moment capacity for an angle without full lateral support, bent about major principal *x*-axis using a moment modification factor (α_m) equal to unity (uniform bending moment distribution)

M_{bx}, M_{by} = (AS/NZS 4600 and AISI) Nominal member moment capacity about the principal *x*- and *y*-axes, respectively

M_e = End bending moment

M_h^* = Design bending moment acting about the *h*-axis parallel to the loaded leg

M_{sx}, M_{sy} = Nominal section moment capacity about the principal *x*- and *y*-axes, respectively

M_x^*, M_y^* = Design bending moments about the principal *x*- and *y*-axes of the effective section, respectively

N_c = Nominal member capacity of the member in compression

N_{ch} = Nominal member capacity in axial compression of a single angle compression member buckling about the *h*-axis parallel to the loaded leg

N_E = Elastic buckling load with respect to the axis of bending

N_s = Nominal section capacity of the member in compression

N^* = Design axial force in the member

r = Radius of gyration

r_h = Radius of gyration about an axis parallel to the loaded leg

S_{hc} = Elastic section modulus for bending about an axis parallel with a leg. Yielding at the loaded leg

S_{ht} = Elastic section modulus for bending about an axis parallel with a leg. Yielding at the tip of the unloaded leg

t = Thickness of the section

Greek Letters

α = Angle between *x*- and *h*-axis (45° for equal angles)

α_{nx}, α_{ny} = Moment amplification factors

β = End moment ratio

δ_b = Moment amplification factor

Appendix C. CURVES OF LOAD VERSUS LATERAL DEFLECTION PERPENDICULAR TO LOADED LEG

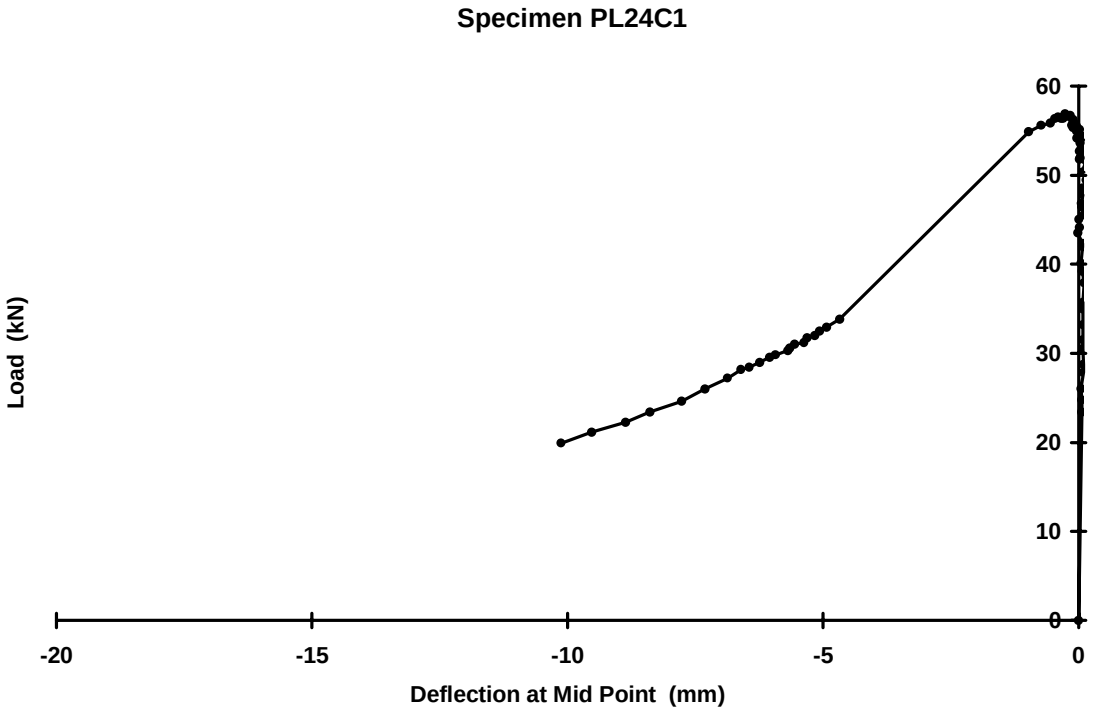

Figure C1 Load Vs Lateral Deflection Specimen PL24C1

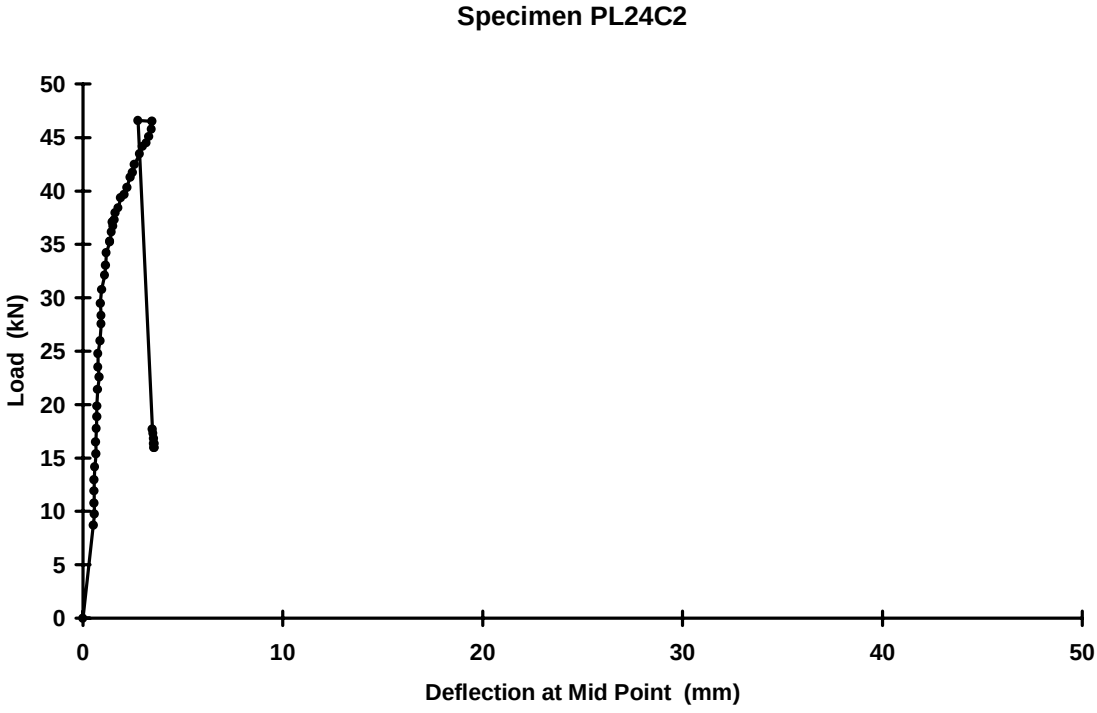

Figure C2 Load Vs Lateral Deflection Specimen PL24C2

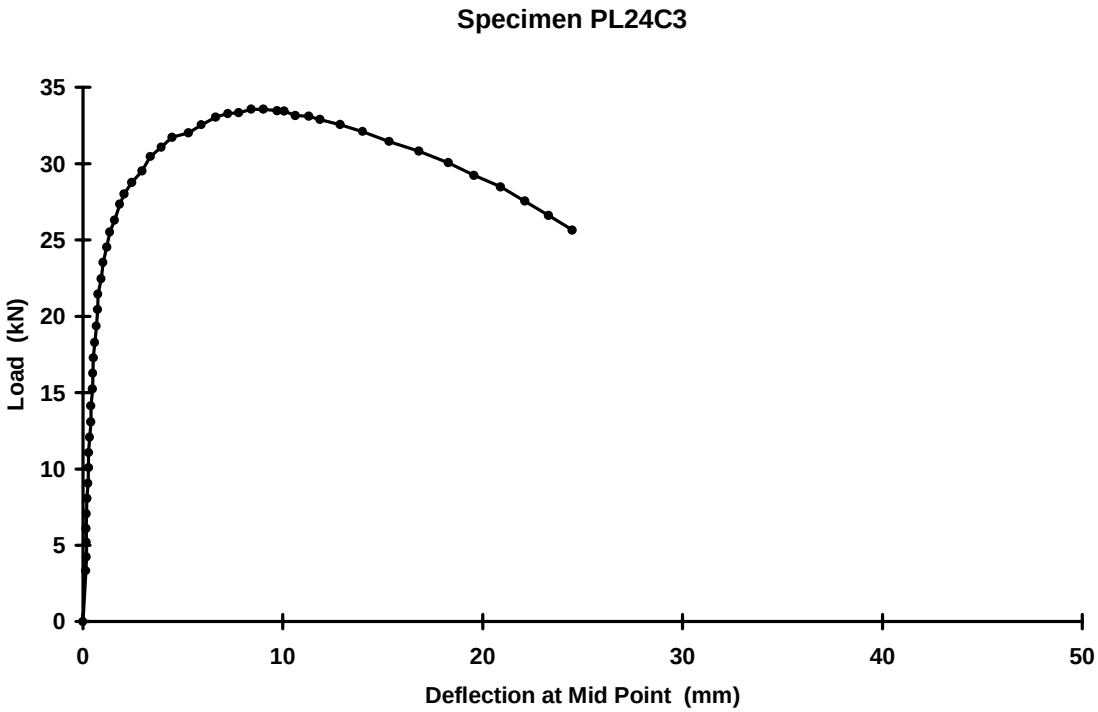

Figure C3 Load Vs Lateral Deflection Specimen PL24C3

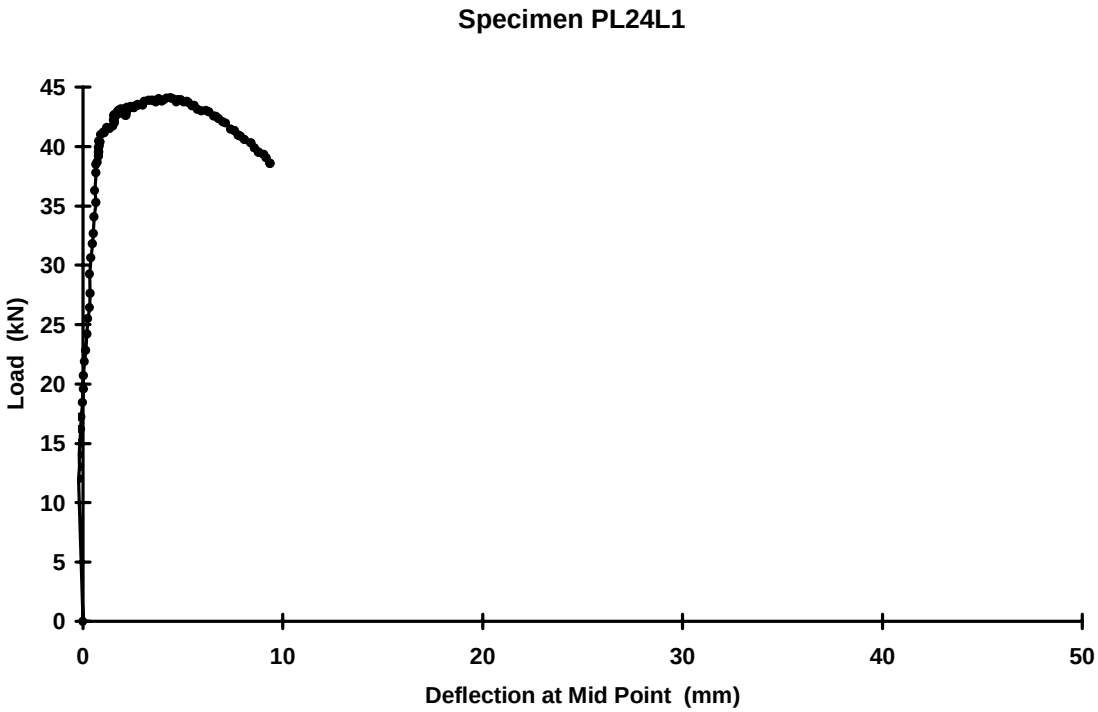

Figure C4 Load Vs Lateral Deflection Specimen PL24L1

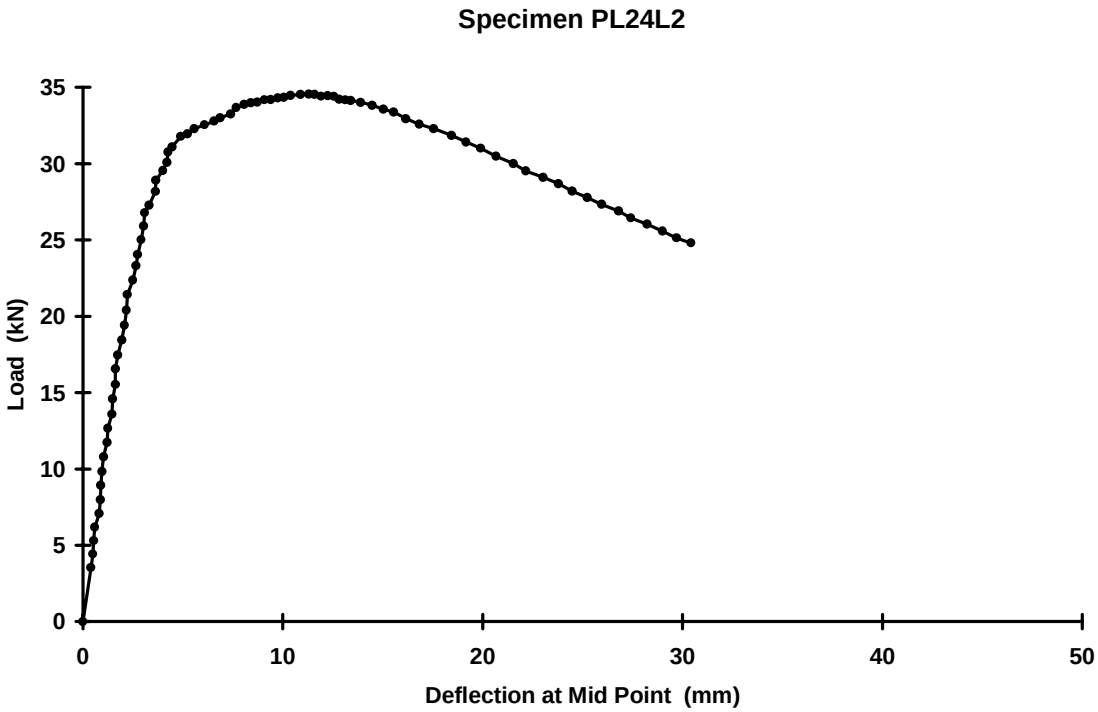

Figure C5 Load Vs Lateral Deflection Specimen PL24L2

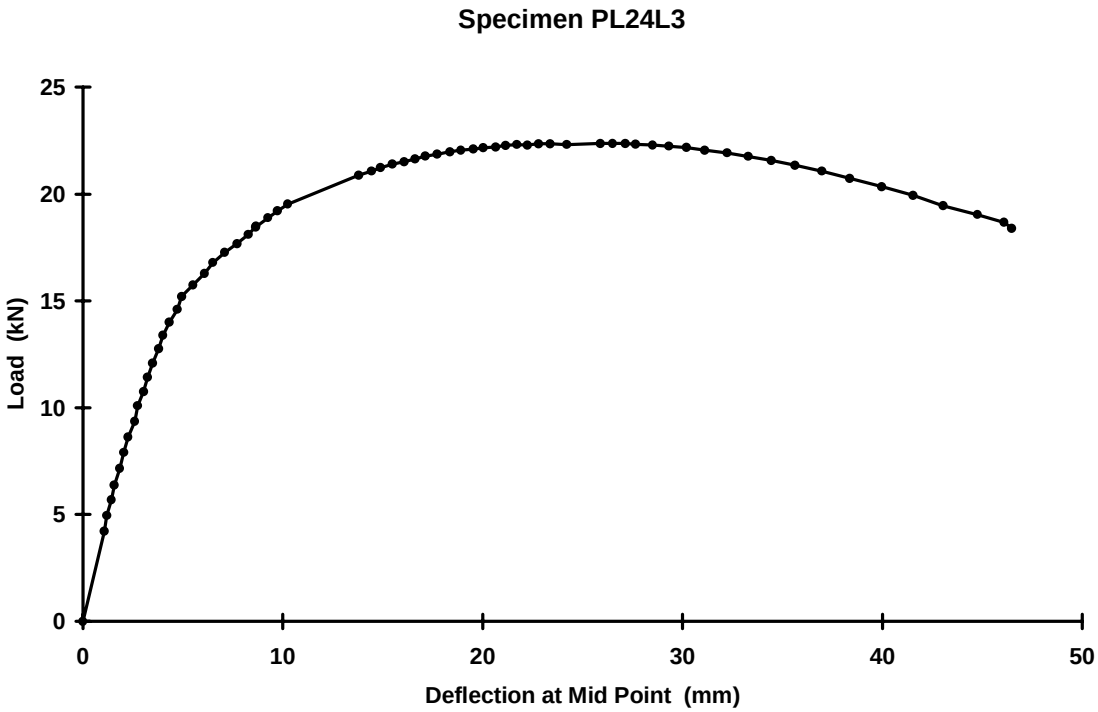

Figure C6 Load Vs Lateral Deflection Specimen PL24L3

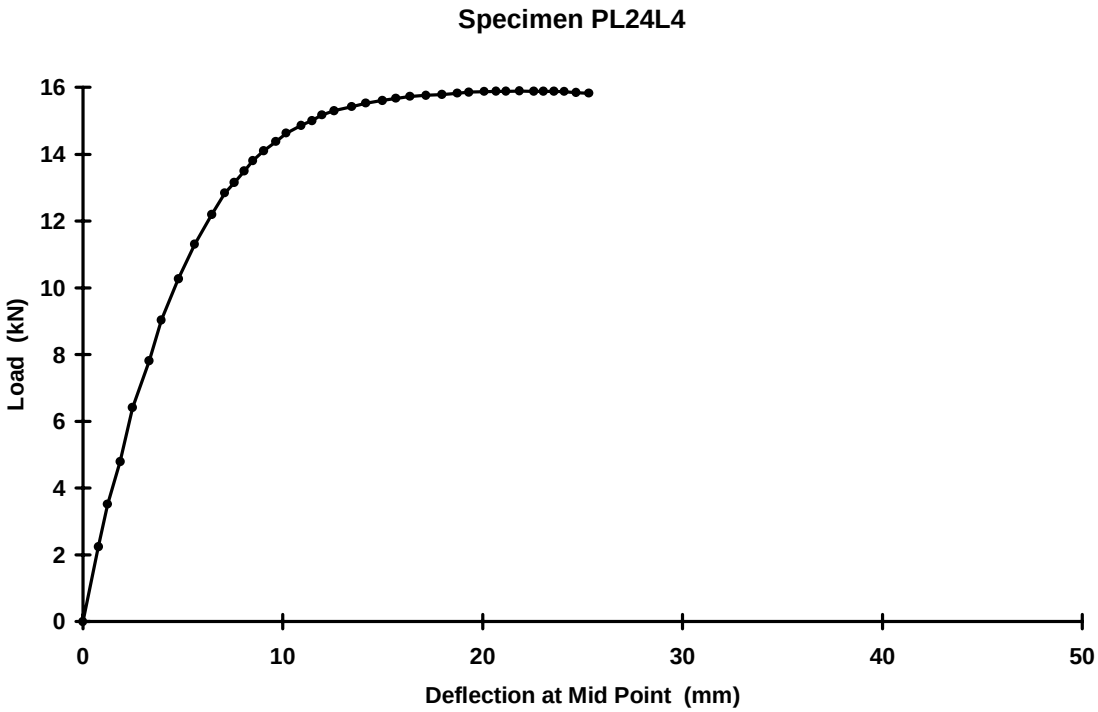

Figure C7 Load Vs Lateral Deflection Specimen PL24L4

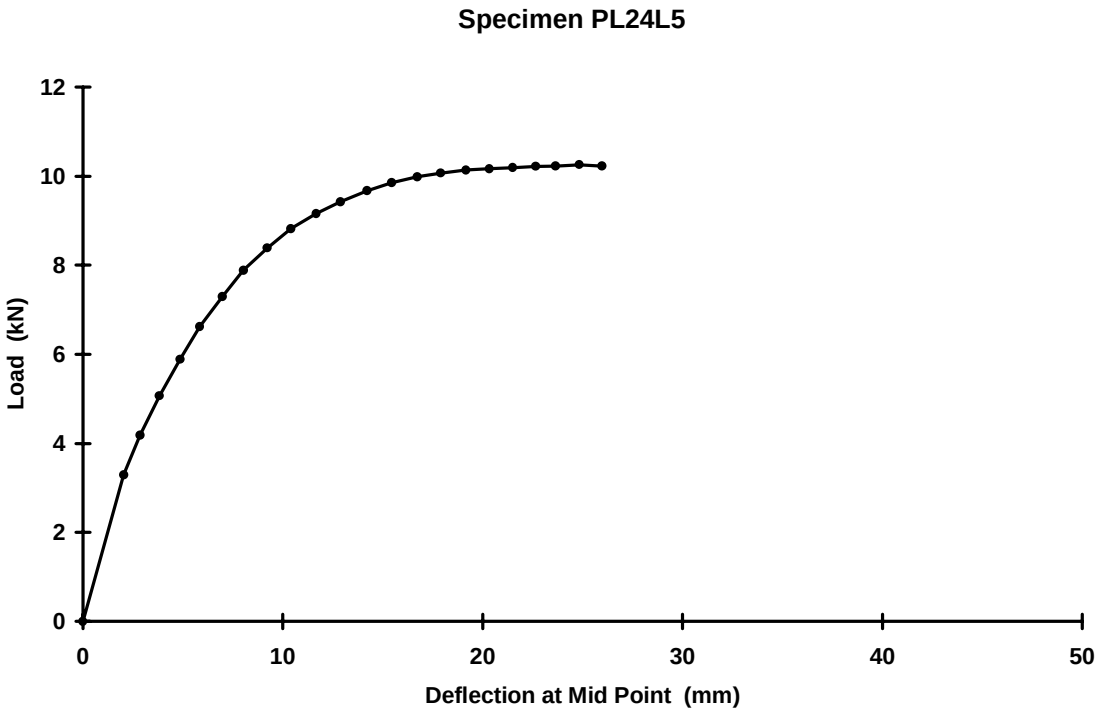

Figure C8 Load Vs Lateral Deflection Specimen PL24L5

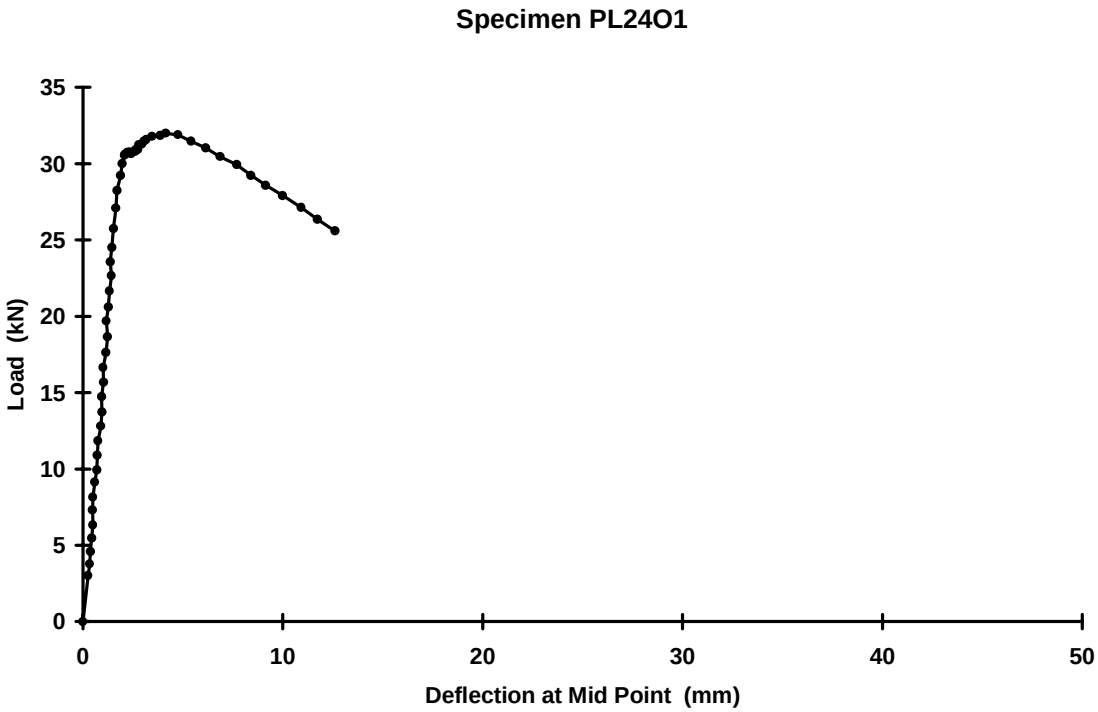

Figure C9 Load Vs Lateral Deflection Specimen PL24O1

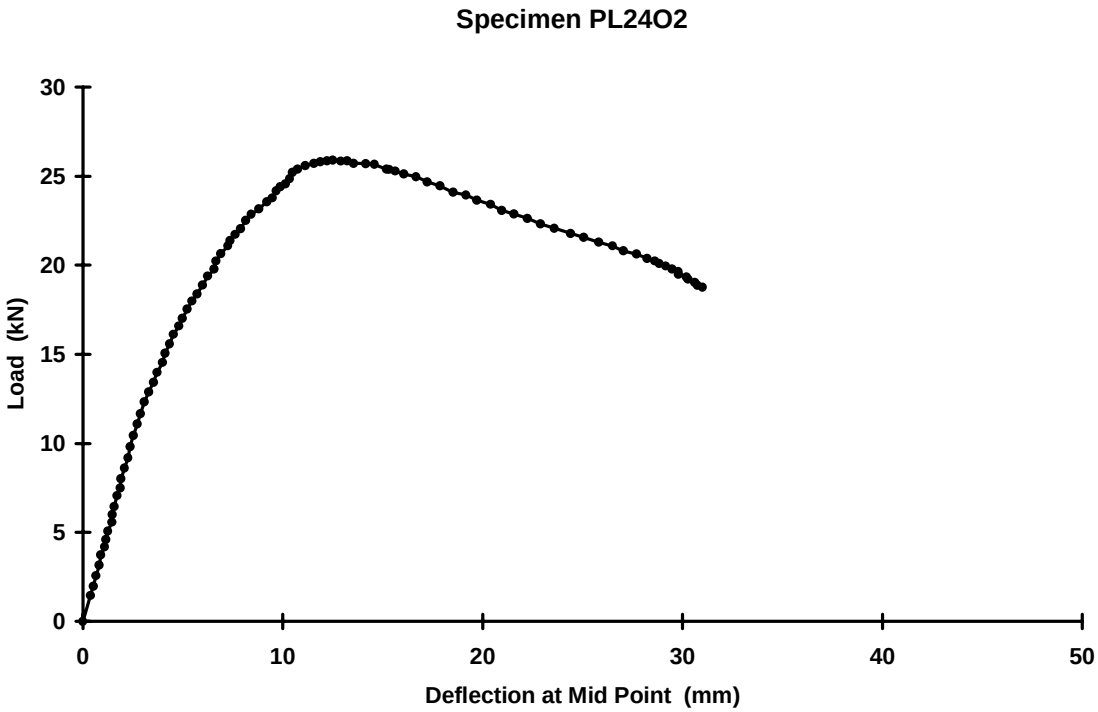

Figure C10 Load Vs Lateral Deflection Specimen PL24O2

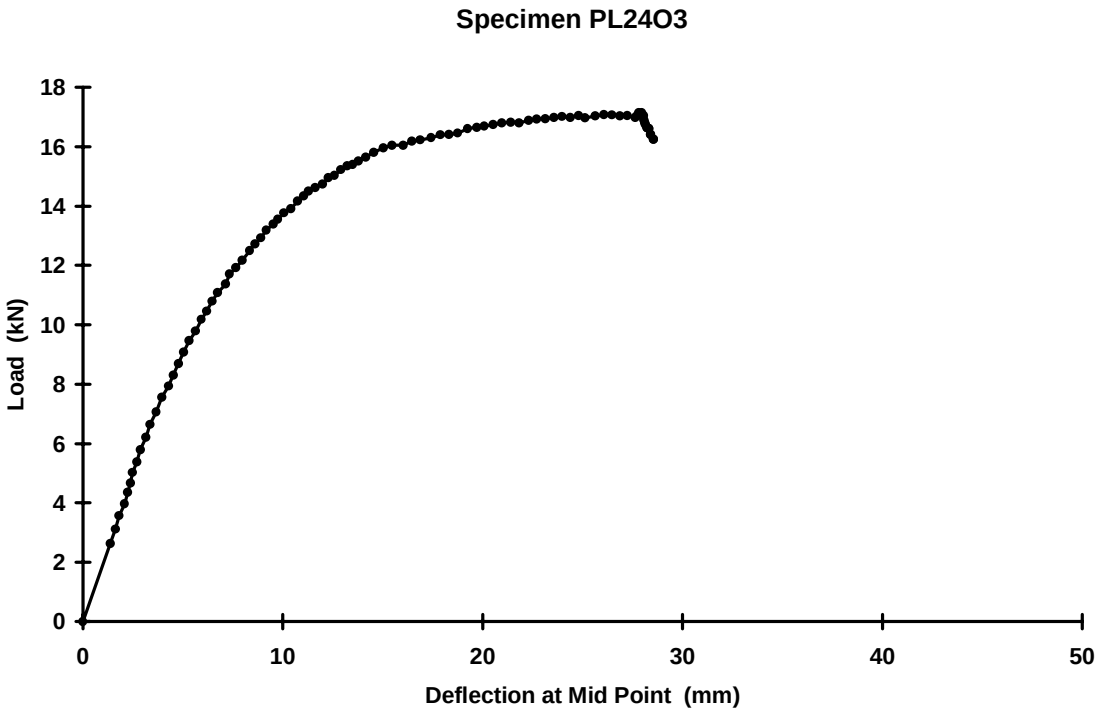

Figure C11 Load Vs Lateral Deflection Specimen PL24O3

Appendix D. CURVES OF LOAD VERSUS TWIST ROTATION AT MID-SPAN

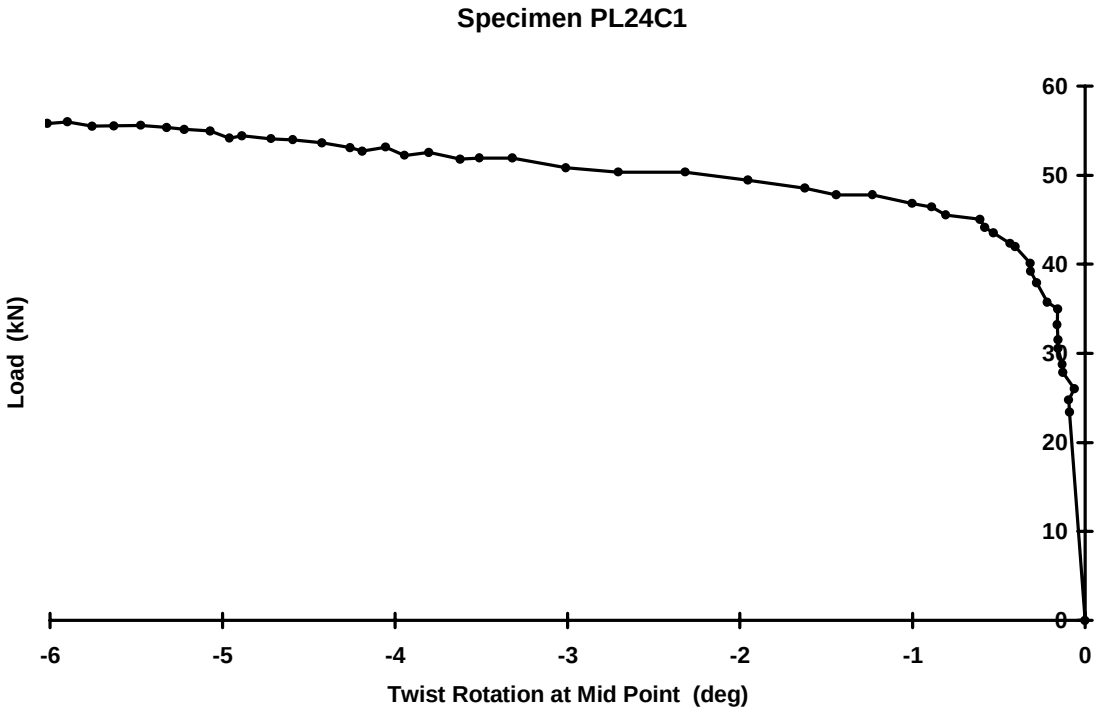

Figure D1 Load Vs Twist Rotation at Mid-Span Specimen PL24C1

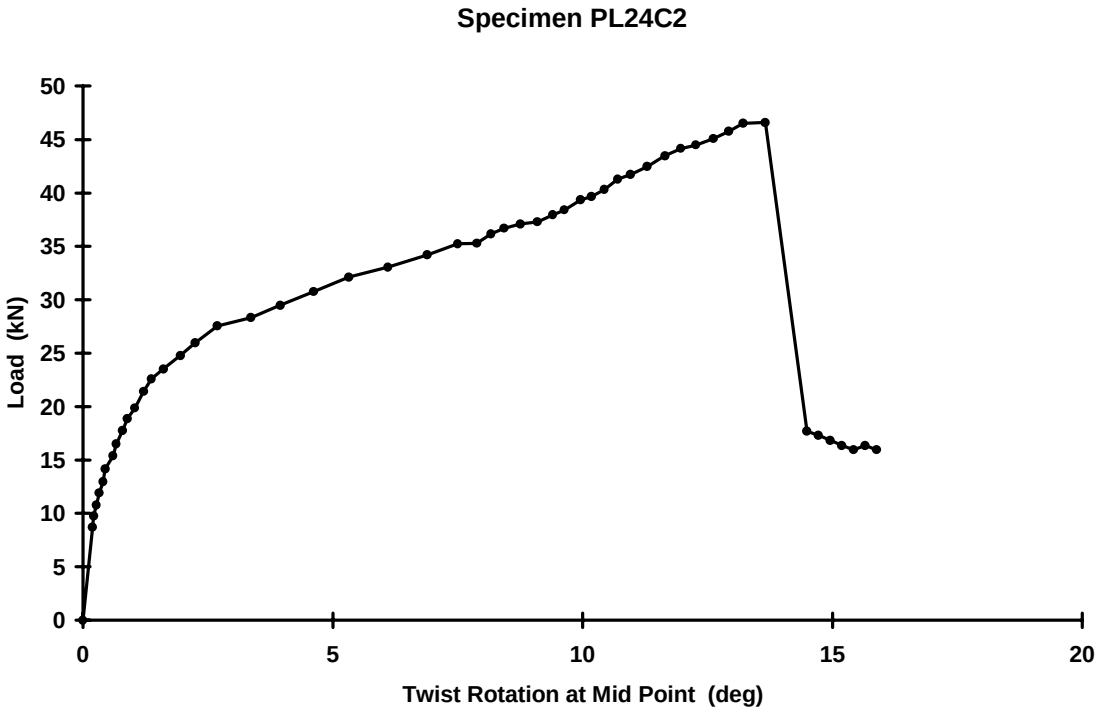

Figure D2 Load Vs Twist Rotation at Mid-Span Specimen PL24C2

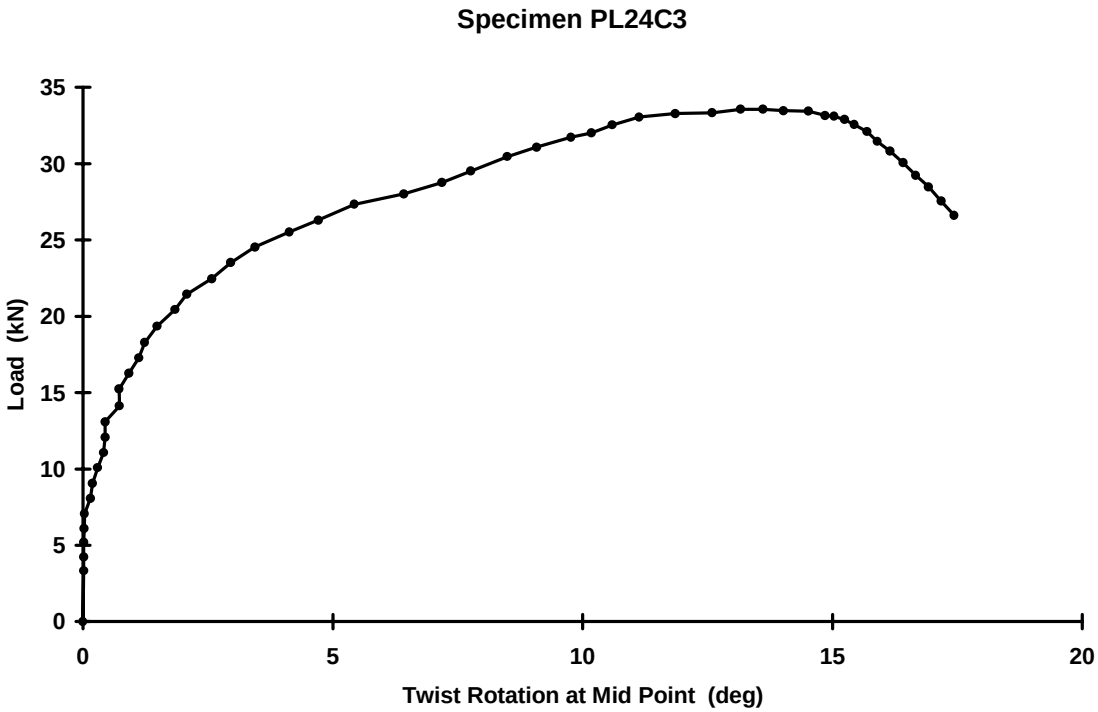

Figure D3 Load Vs Twist Rotation at Mid-Span Specimen PL24C3

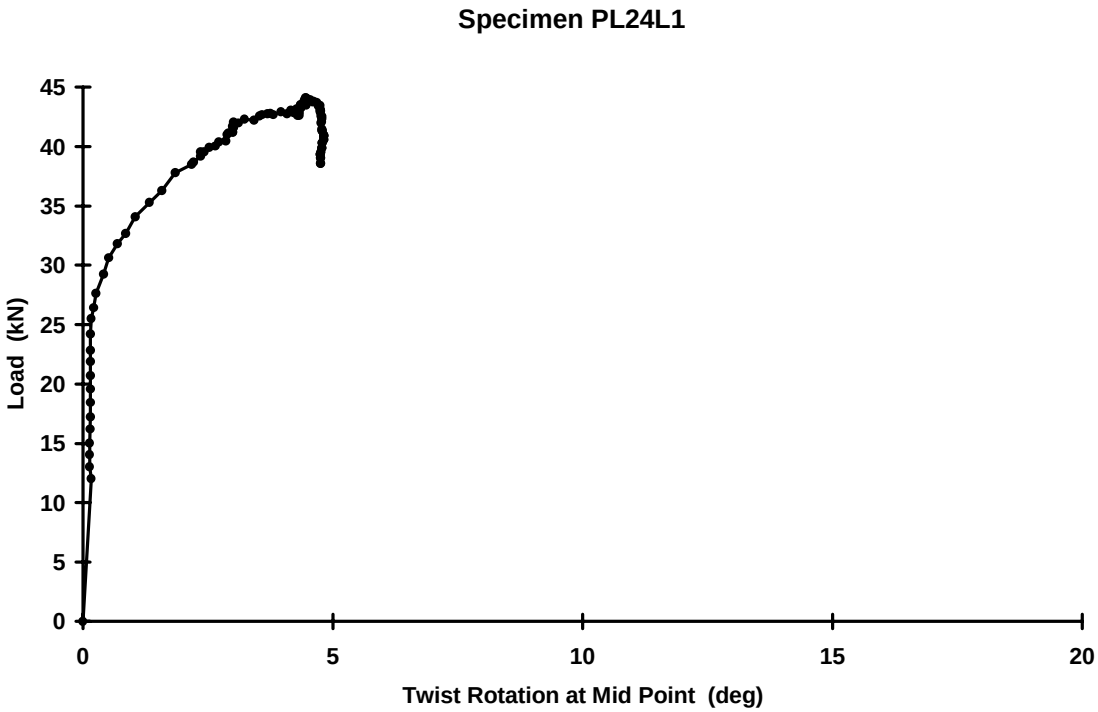

Figure D4 Load Vs Twist Rotation at Mid-Span Specimen PL24L1

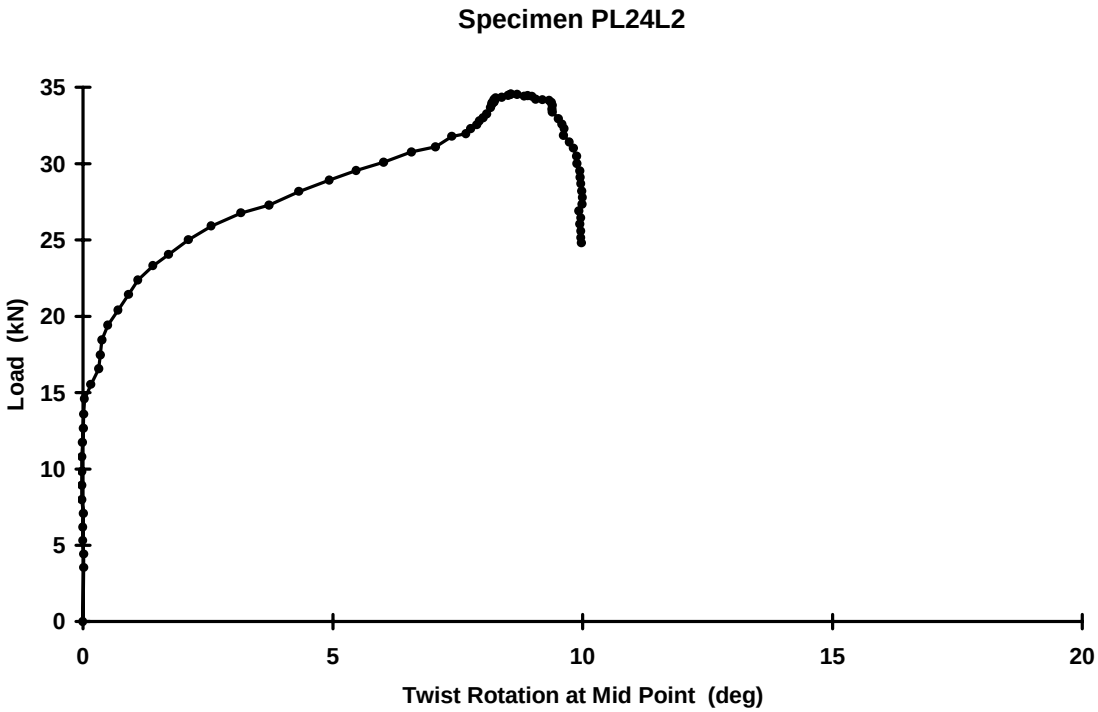

Figure D5 Load Vs Twist Rotation at Mid-Span Specimen PL24L2

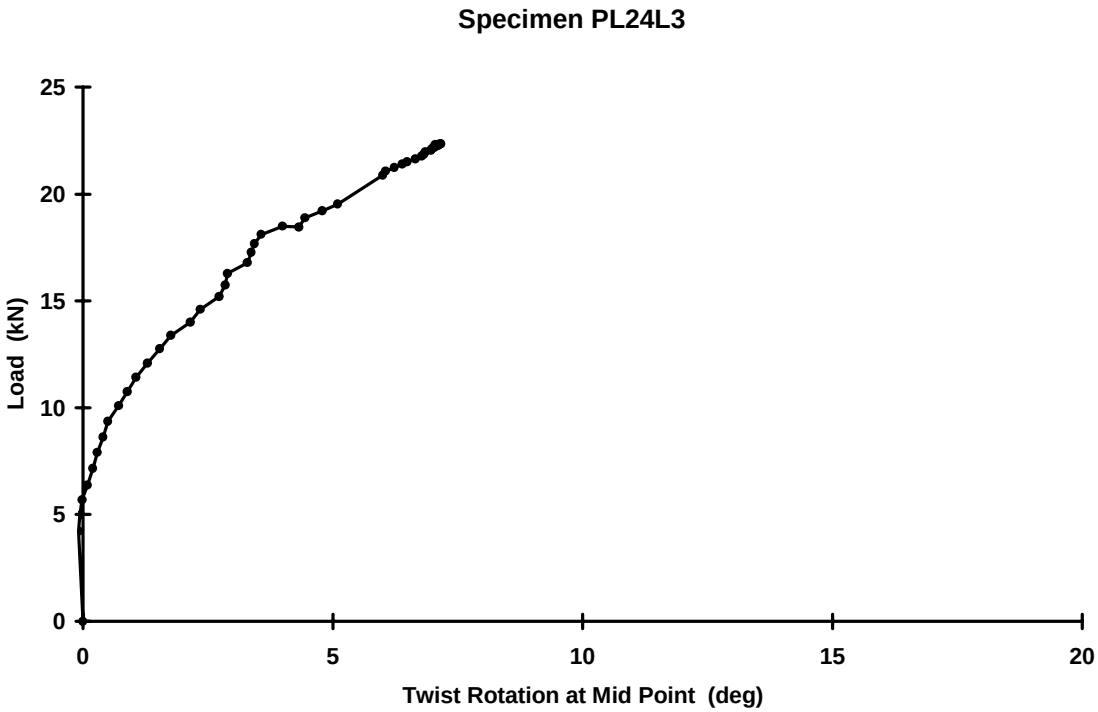

Figure D6 Load Vs Twist Rotation at Mid-Span Specimen PL24L3

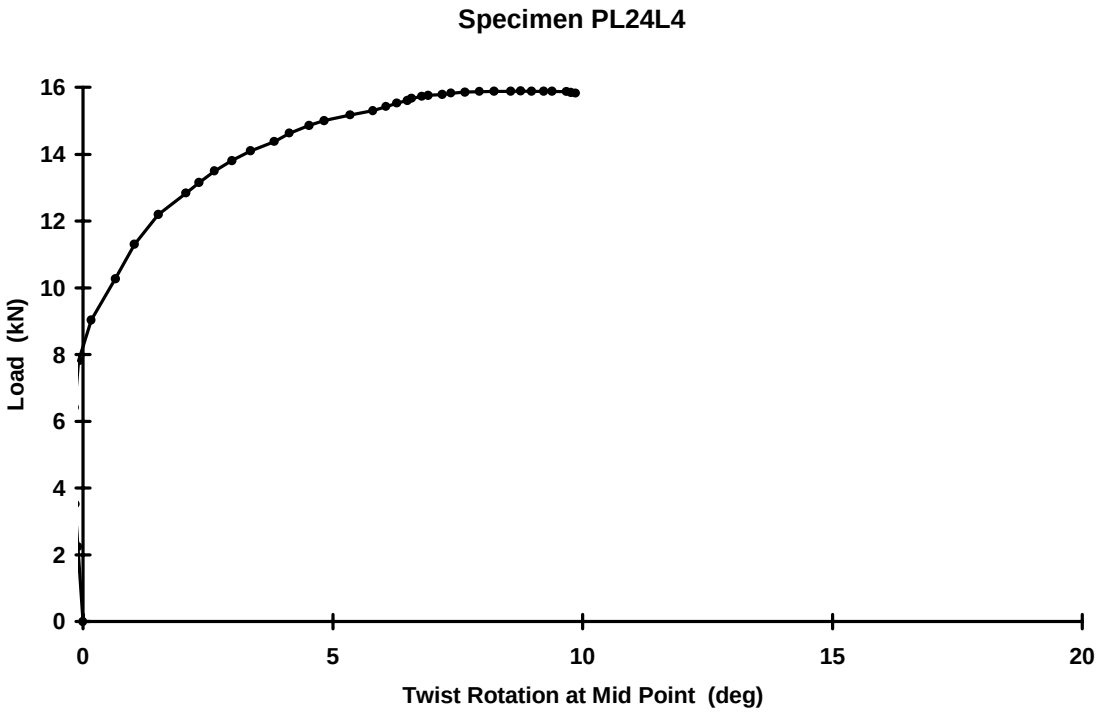

Figure D7 Load Vs Twist Rotation at Mid-Span Specimen PL24L4

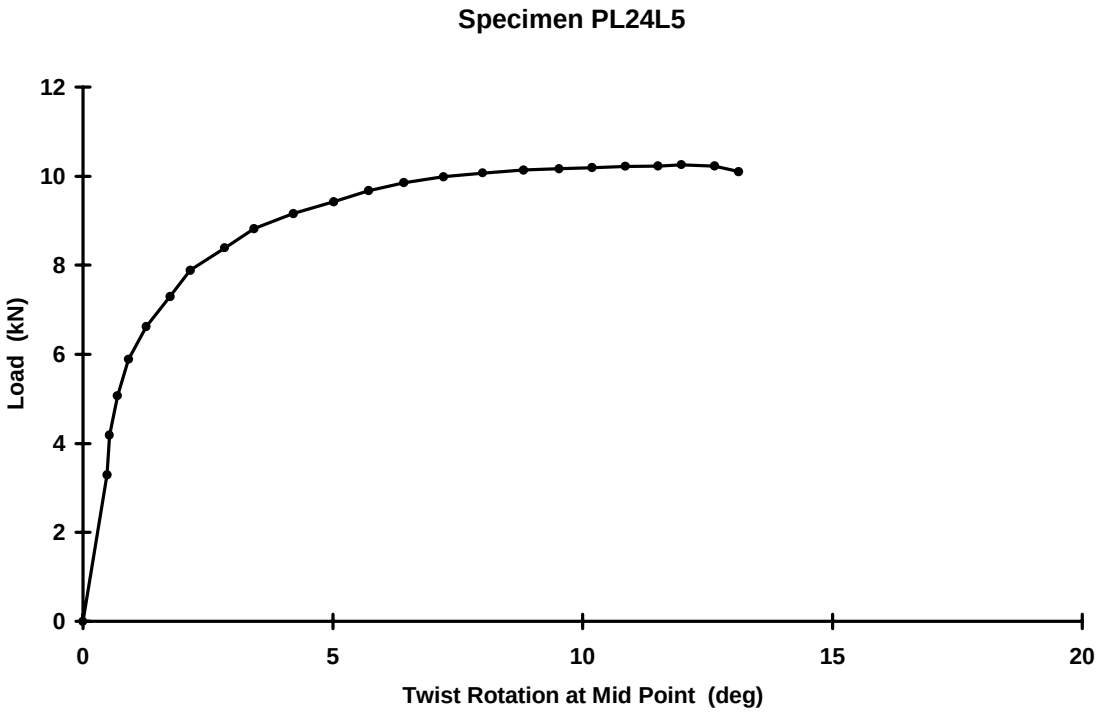

Figure D8 Load Vs Twist Rotation at Mid-Span Specimen PL24L5

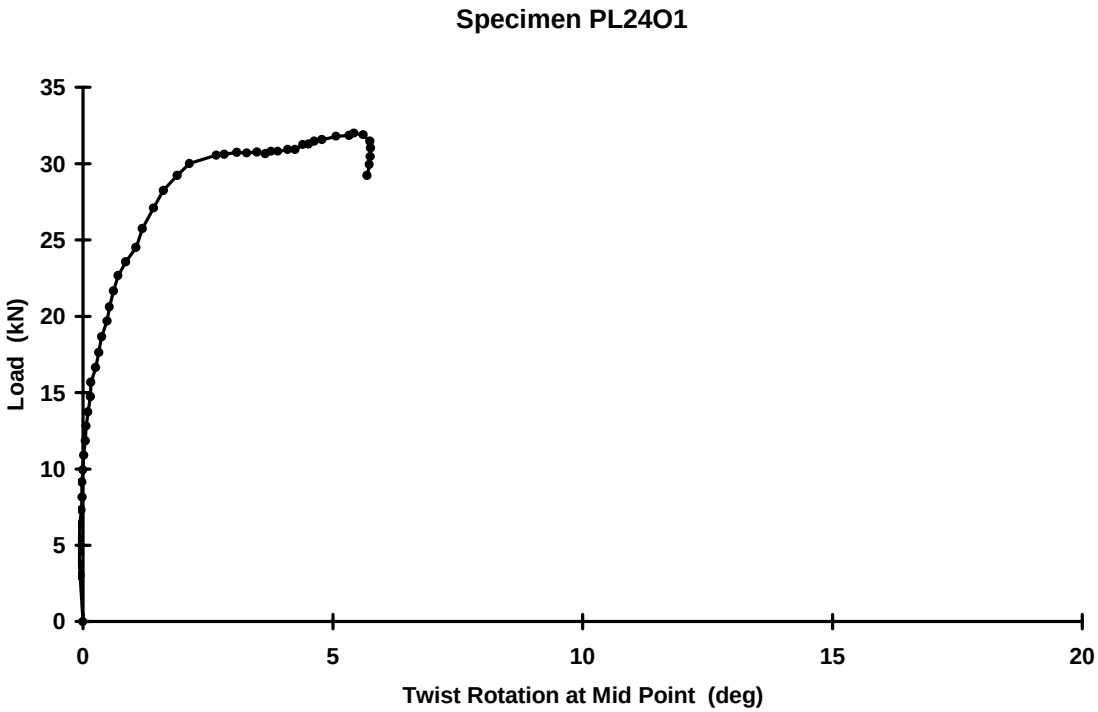

Figure D9 Load Vs Twist Rotation at Mid-Span Specimen PL24O1

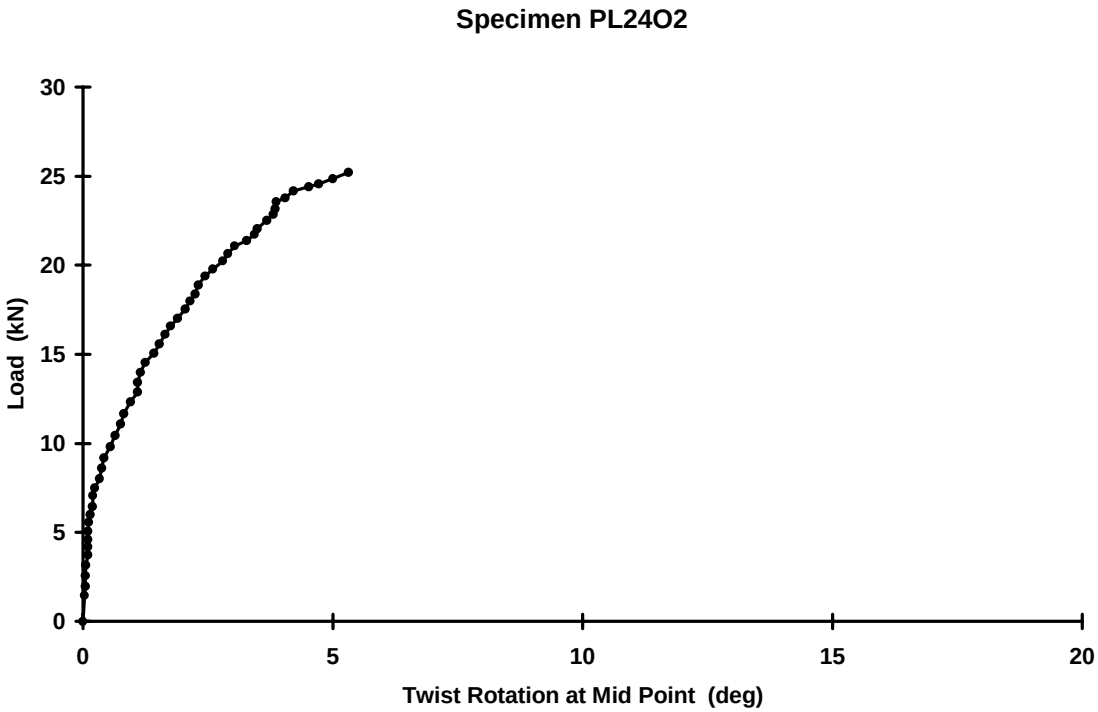

Figure D10 Load Vs Twist Rotation at Mid-Span Specimen PL24O2

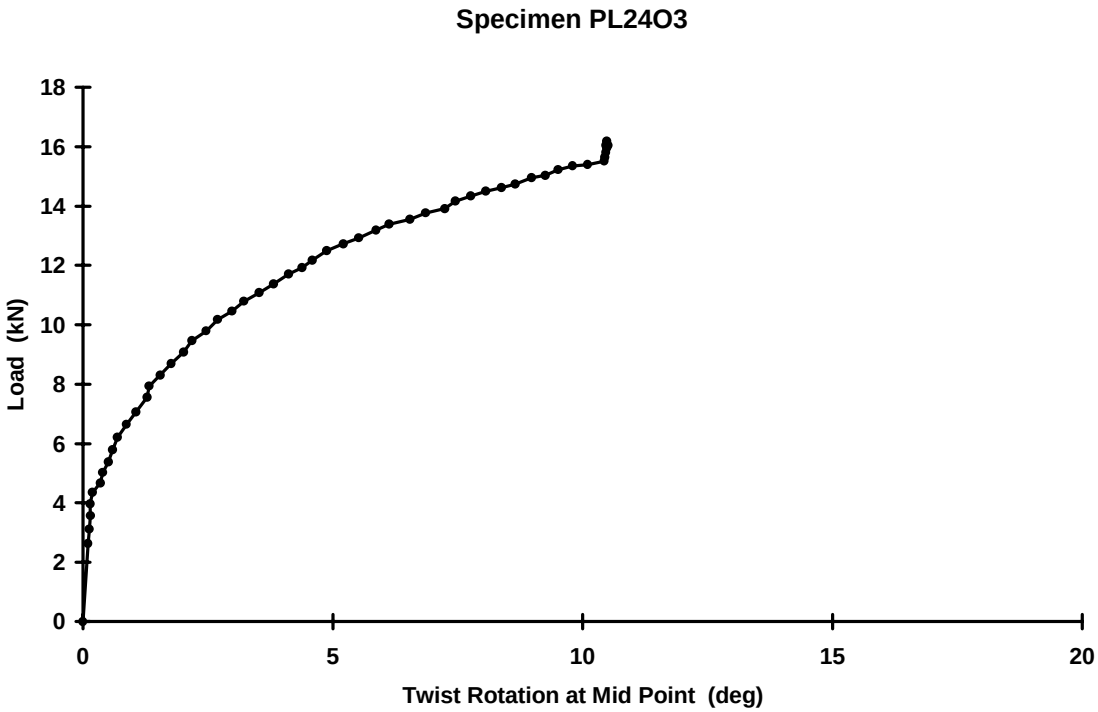

Figure D11 Load Vs Twist Rotation at Mid-Span Specimen PL24O3

Appendix E. CURVES OF LOAD VERSUS ROTATION OF END BEARINGS

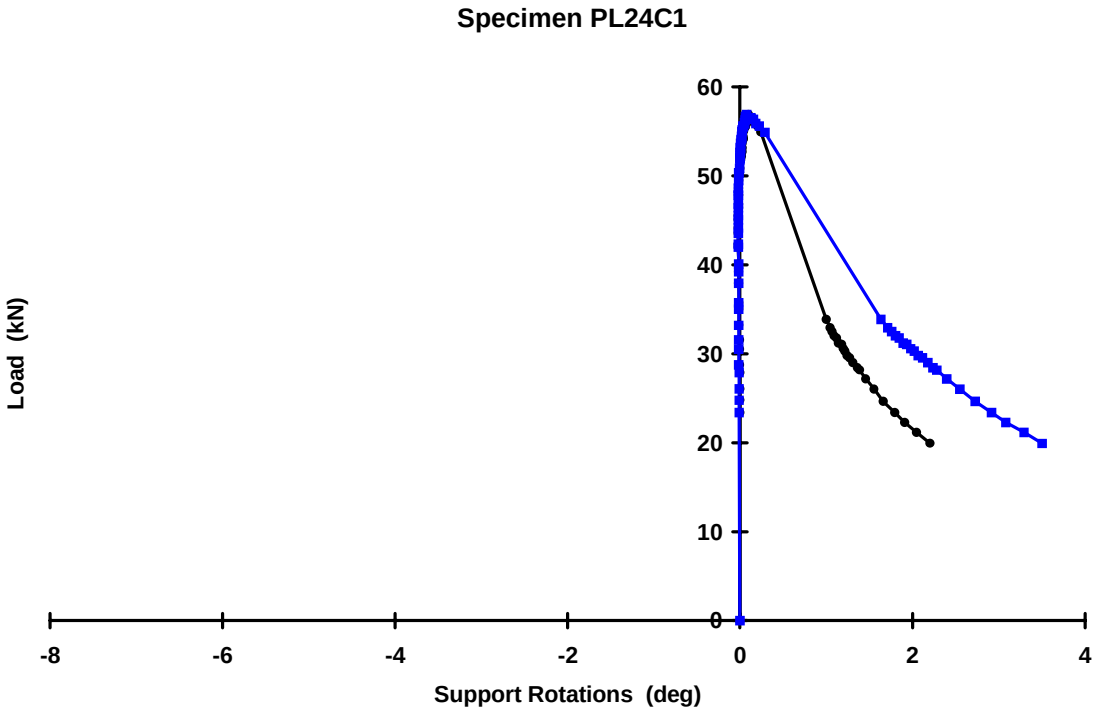

Figure E1 Load Vs Rotation of End Bearings Specimen PL24C1

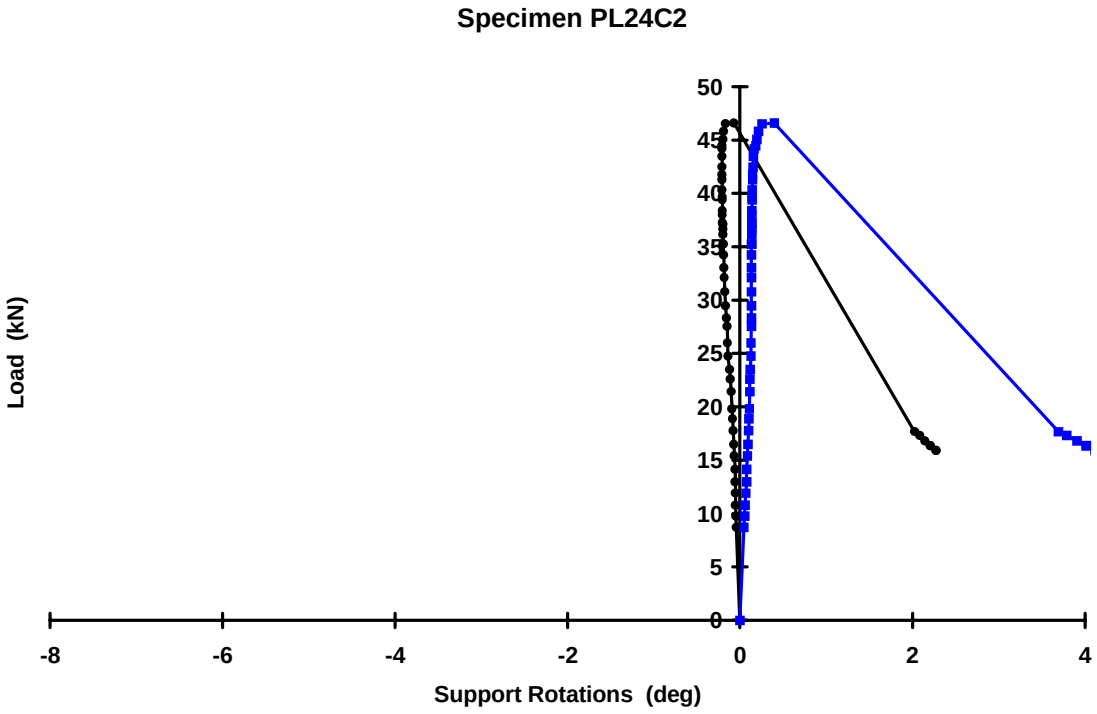

Figure E2 Load Vs Rotation of End Bearings Specimen PL24C2

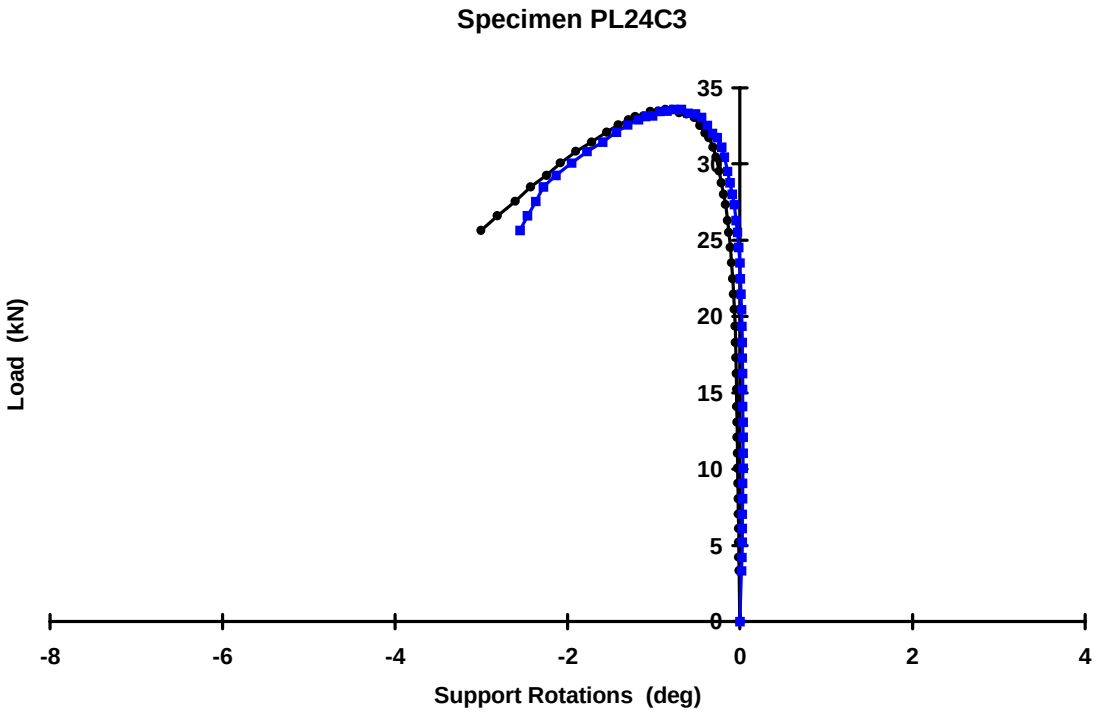

Figure E3 Load Vs Rotation of End Bearings Specimen PL24C3

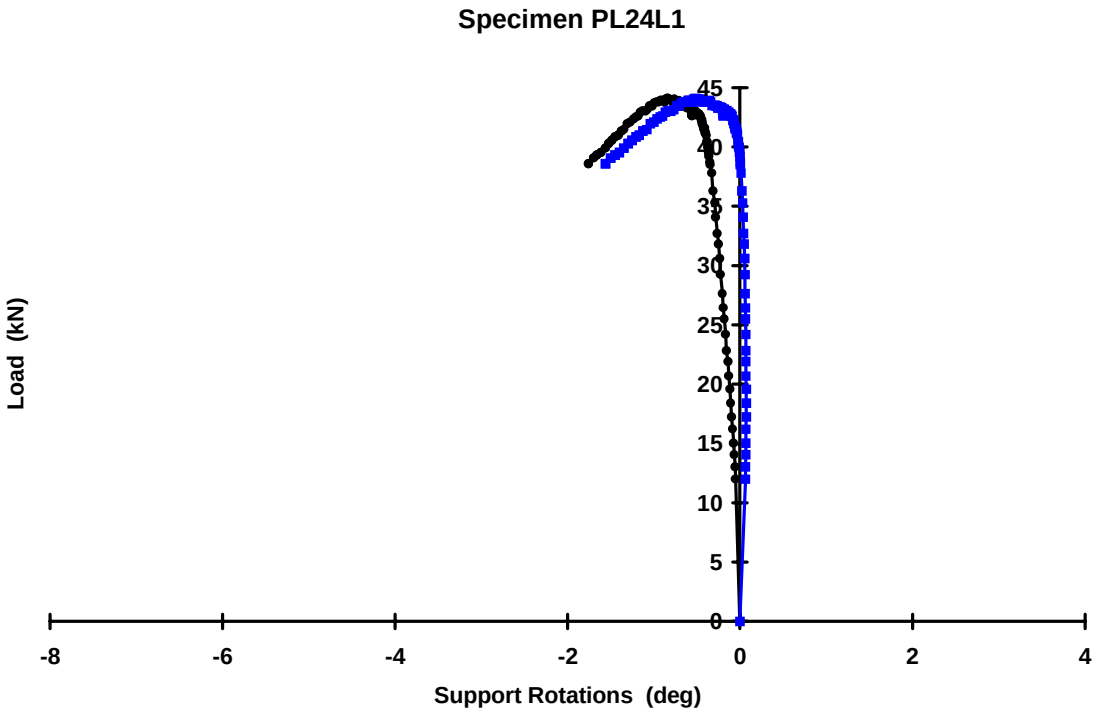

Figure E4 Load Vs Rotation of End Bearings Specimen PL24L1

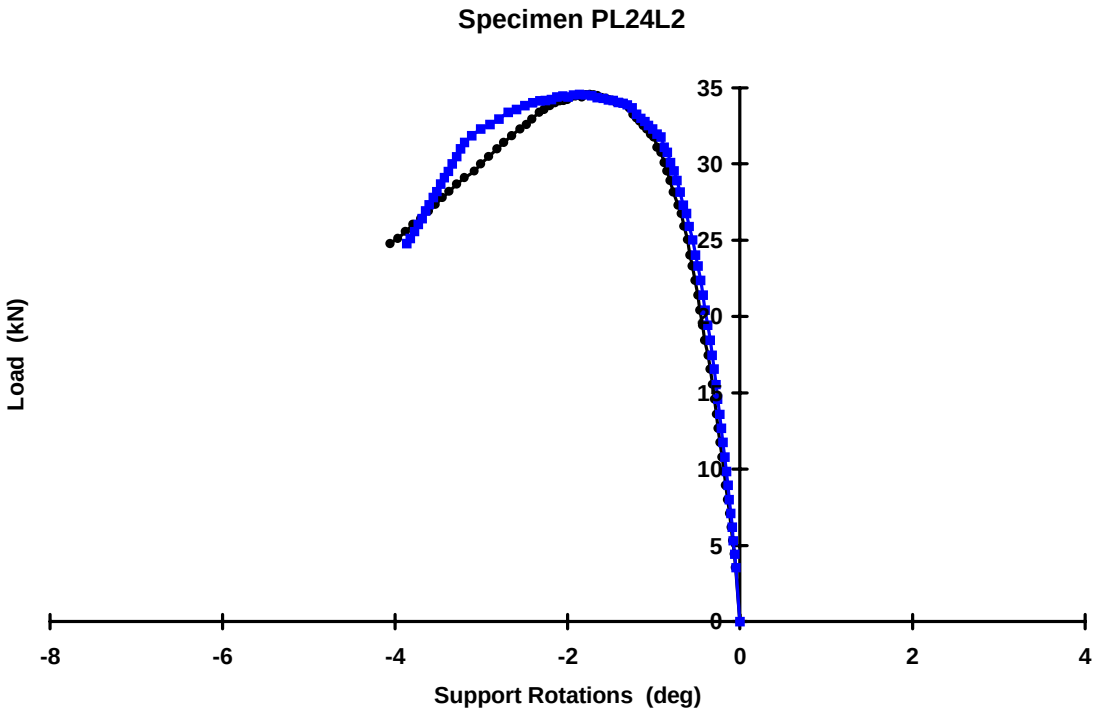

Figure E5 Load Vs Rotation of End Bearings Specimen PL24L2

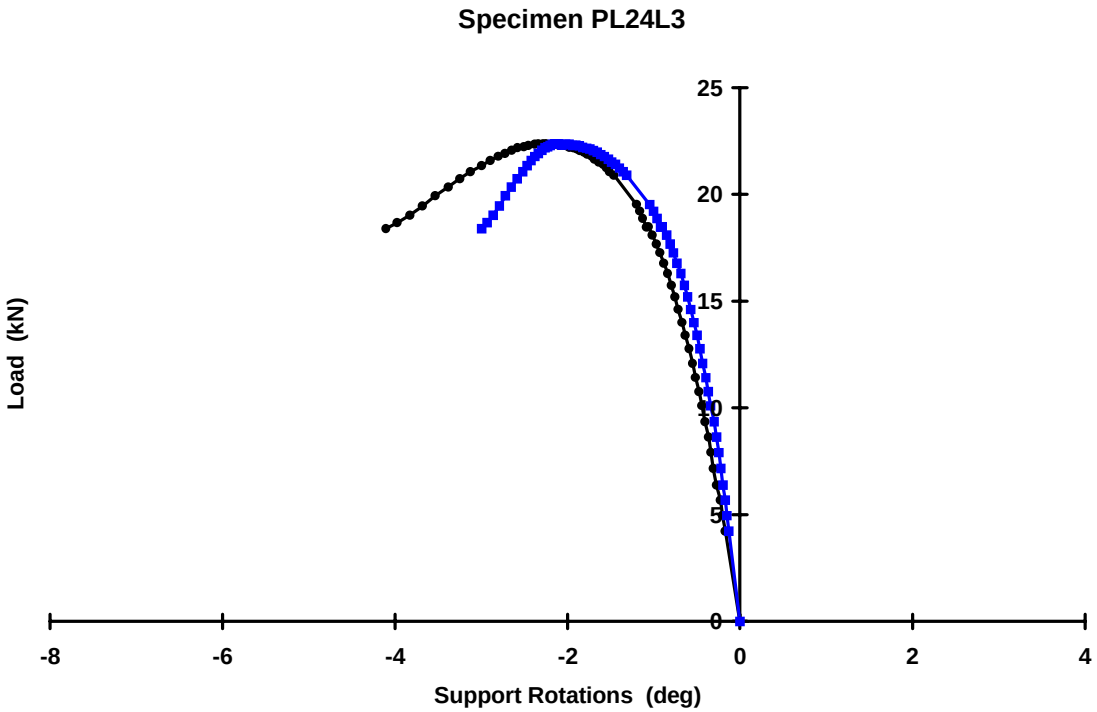

Figure E6 Load Vs Rotation of End Bearings Specimen PL24L3

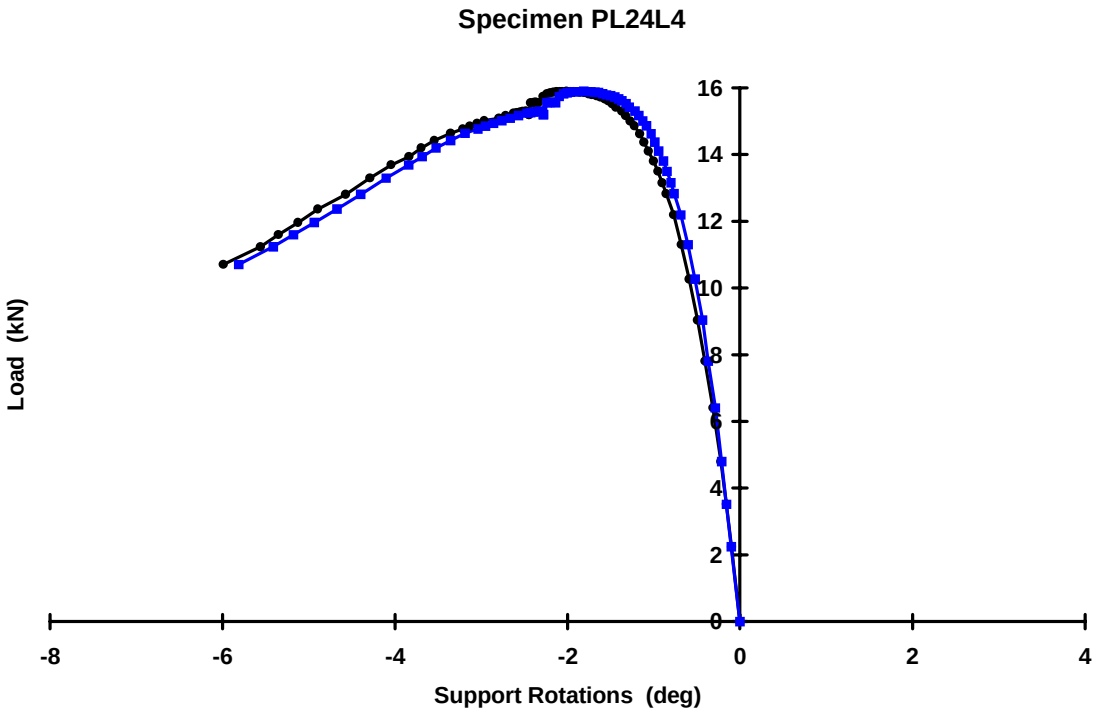

Figure E7 Load Vs Rotation of End Bearings Specimen PL24L4

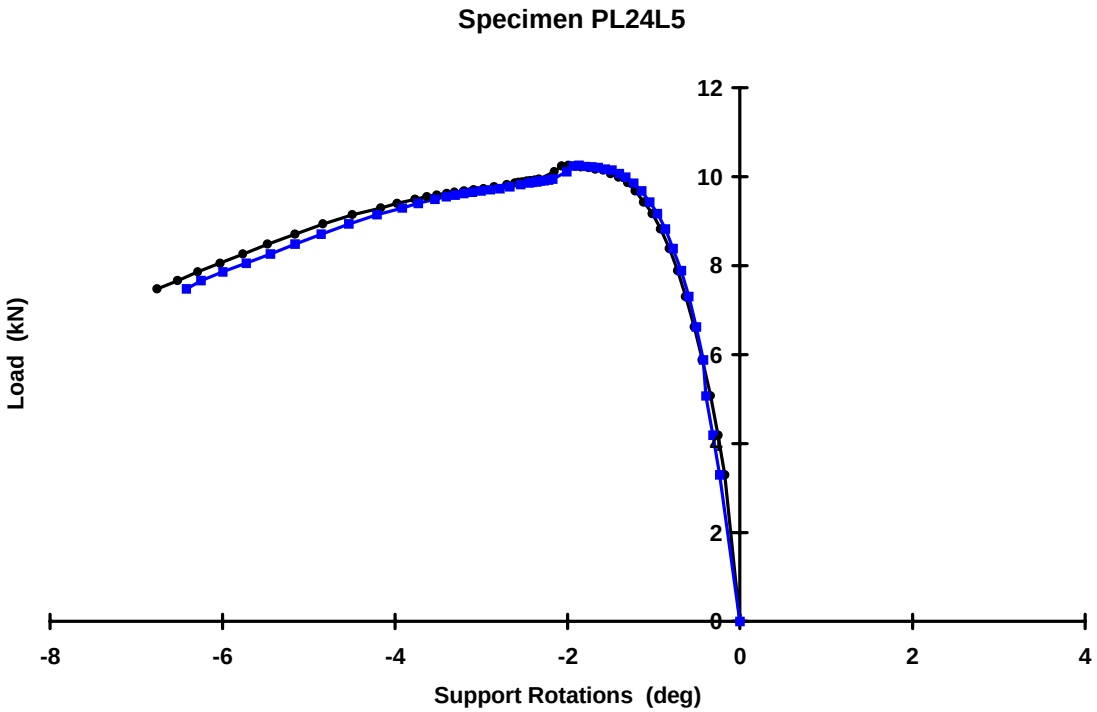

Figure E8 Load Vs Rotation of End Bearings Specimen PL24L5

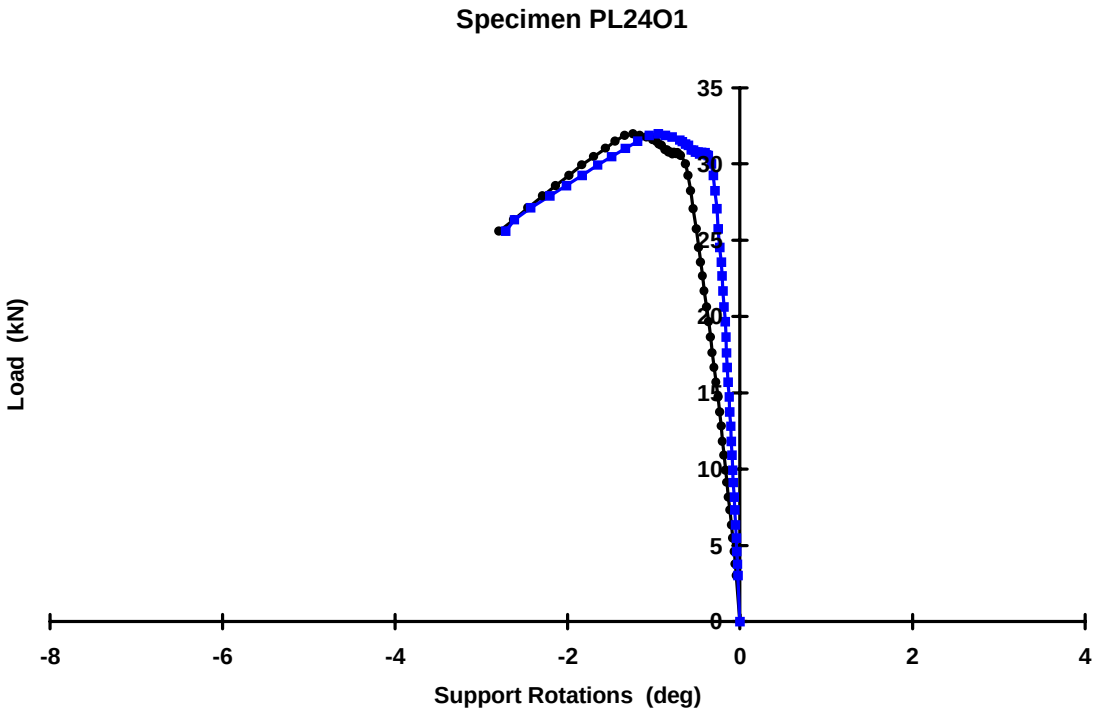

Figure E9 Load Vs Rotation of End Bearings Specimen PL24O1

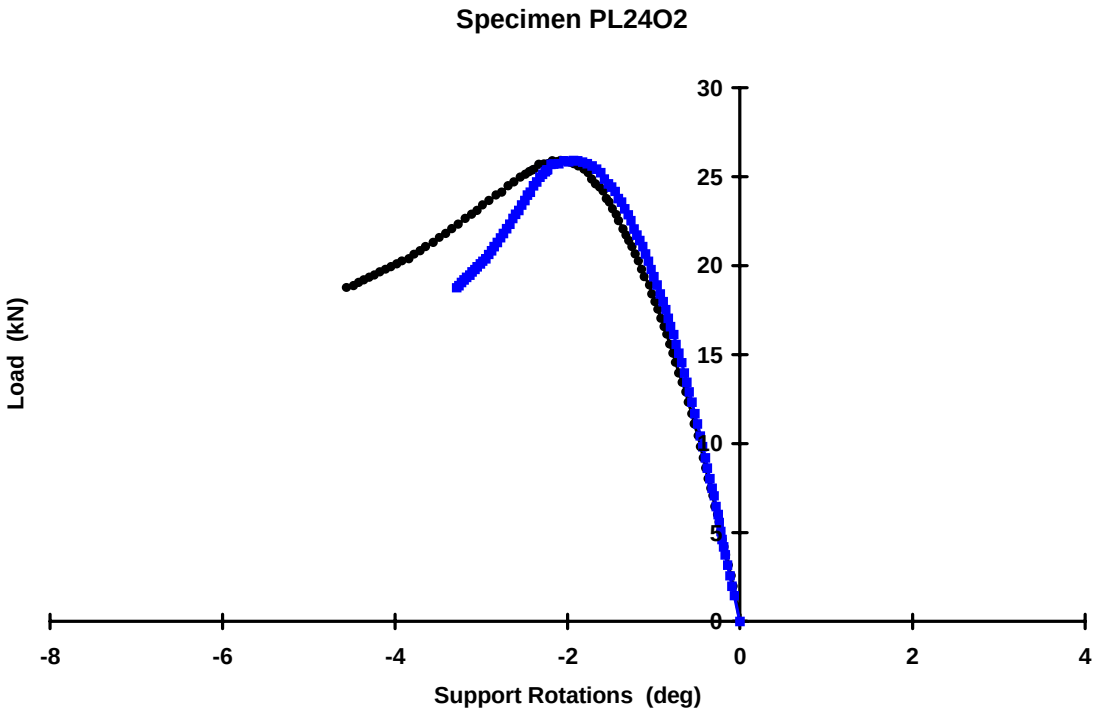

Figure E10 Load Vs Rotation of End Bearings Specimen PL24O2

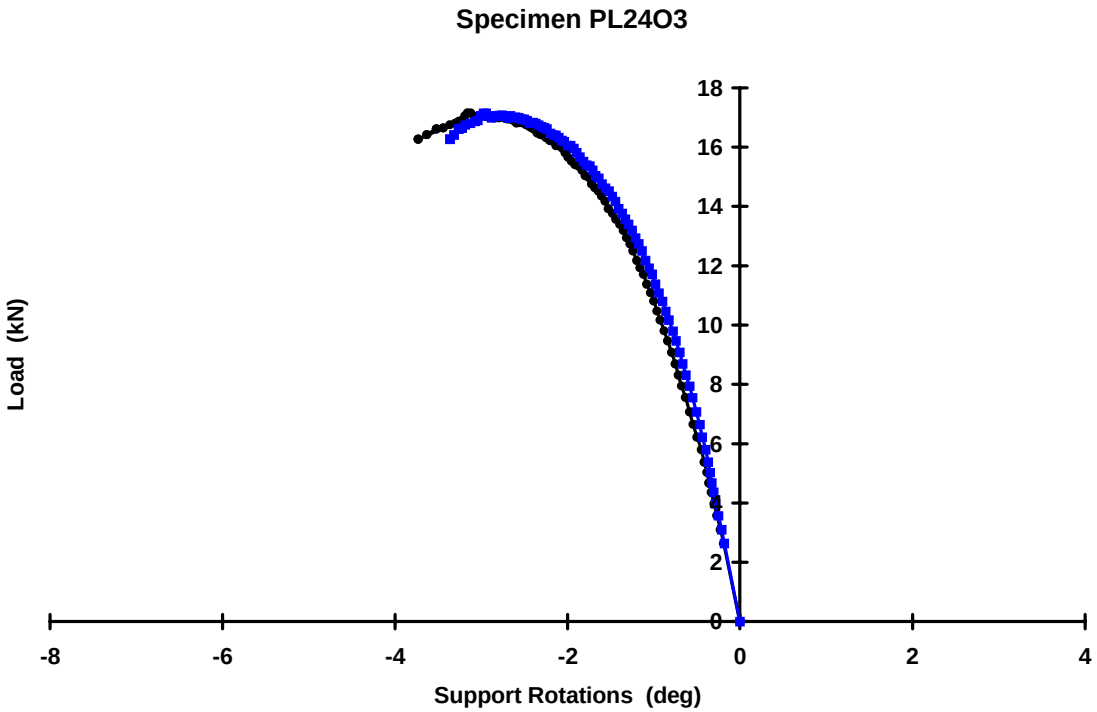

Figure E11 Load Vs Rotation of End Bearings Specimen PL24O3